# Reduced kinetic mechanisms of diesel fuel surrogate for engine CFD simulations

Alessio Frassoldati [a,*], Gianluca D'Errico [b], Tommaso Lucchini [b], Alessandro Stagni [a], Alberto Cuoci [a], Tiziano Faravelli [a], Angelo Onorati [b], Eliseo Ranzi [a]

[a] *Department of Chemistry, Materials, and Chemical Engineering "G. Natta", Politecnico di Milano, P.zza Leonardo da Vinci 32, 20133 Milano, Italy*
[b] *Department of Energy, Politecnico di Milano, via Lambruschini 4, 20156 Milano, Italy*

Received 19 March 2015
Revised 27 July 2015
Accepted 28 July 2015
Available online 19 August 2015

## 1. Introduction

Diesel engines will remain for several decades one of the most important powertrain technologies for transportation [1,2]. However, to fulfill the requirements in terms of pollutant reduction and efficiency increase, different solutions are investigated, such as new combustion strategies and alternative fuels. Within this context, detailed numerical tools and reliable kinetic modeling of combustion are required [2], for a proper prediction of engine efficiency and pollutants (PAH, soot, $NO_x$, etc.). The description of the combustion process for the liquid fuels employed in transportations is a very complex task for two different reasons: the challenging characterization of the complex mixture of several hydrocarbon isomers, and the complexity of the oxidation mechanisms of large hydrocarbon and oxygenated molecules [3]. While surrogate mixtures of reference components allow to tackle the first difficulty [4,5], the complex behavior of the oxidation mechanisms is mostly overcome by adopting a lumping approach [6,7].

Multi-dimensional simulations are now widely employed to design and develop direct-injection diesel engines. Most of the attention is focused on the combustion phase, due to the need to reduce pollutant emissions and increase thermal efficiency. To this aim, both standard and advanced combustion modes are widely studied, analyzing how fuel distribution and flame structure are affected by injection strategy, fuel composition, mixture, and thermal stratification [8–12]. However, the use of multiple injections and engine operation under advanced combustion modes involves a large variety of combustion regimes where fuel auto-ignition and flame propagation take place in a wide range of pressures, temperatures, and equivalence ratio conditions. Hence, realistic results can be achieved only if both complex fuel chemistry and its interaction with turbulence are properly taken into account inside a Computational Fluid Dynamics (CFD) simulation. These reasons justify the interest towards the development of skeletal kinetic models, especially considering that the

* Corresponding author.
*E-mail address:* alessio.frassoldati@polimi.it (A. Frassoldati).

computational cost scales by the second/third power of the number of species and that the very large sizes of detailed kinetic schemes could pose problems even in 1-D modeling [13].

Due to the similarity between $nC_{12}H_{26}$ and diesel fuel in terms of liquid and chemical properties, several spray combustion experiments were carried out in the SANDIA constant-volume vessel by using neat n-dodecane at different oxygen concentration. These data are publicly available through the Engine Combustion Network (www.ca.sandia.gov/ecn). All these reasons explain the interest towards the development of a skeletal kinetic model of n-dodecane oxidation.

In the following, different skeletal n-dodecane kinetic mechanisms are first investigated in ideal reactors, where reactivity is controlled only by chemical kinetics, in order to understand their characteristics, peculiarities and reliability in different operating conditions. These mechanisms are then further validated in comparison to measurements of 1D laminar flames and isolated fuel droplets in microgravity conditions, where diffusion also plays an important role. All these comparisons allow to better discuss the differences observed when these mechanisms are adopted in the modeling of more complex systems, where the use of CFD codes prevents detailed chemi-cal analyses. Finally, paragraph 5 compares the predictions of these kinetic schemes in diesel-like spray conditions, using an unsteady flamelet based approach to model the turbulent non-premixed flame. Alternative and more complex turbulent combustion models could be adopted with the proposed skeletal kinetic mechanism, but their comparison is out of the scopes of the present investigation.

## 2. Mechanism reduction: skeletal mechanism of n-dodecane oxidation

The kinetic modeling of the autoignition of hydrocarbon fuels in typical engine conditions requires a careful analysis of both low and high-temperature mechanisms. A general detailed kinetic scheme (POLIMI_TOT_1407) (http://creckmodeling.chem.polimi.it/), consisting of more than 450 species and ~15,000 reactions, was discussed in previous papers [6,14]. This comprehensive kinetic scheme is based on a detailed core mechanism of C1–C4-species, a lumped description of the primary propagation reactions of larger species and their primary intermediates, and permits description of the oxidation of hydrocarbons up to jet and diesel fuels, including also alcohols and biodiesel fuels [15]. This approach, together with an extensive use of structural analogies and similarities within the different reaction classes, easily allows extension of the scheme to new species [16].

This general kinetic model has been validated in a wide range of operating conditions through the comparison with experimental measurements carried out in well controlled reaction environments (jet stirred reactors, rapid compression machines, shock tubes, flow reactors, etc) [17–19], covering both high [15] and low temperature [6,14] conditions. The comprehensive validation proved the reliability of the mechanism in all the conditions relevant to engine combustion. The same kinetic scheme, which is also capable of simulat-ing the combustion behavior of real transportation fuels [19,20], has been also successfully applied to the evaluation of the auto-ignition propensities of different fuel surrogate mixtures in SI and HCCI engines over a wide set of operating condition, as discussed in previous works [21–24].

Starting from this kinetic scheme (POLIMI_TOT_1407), a skeletal mechanism (Polimi_NC12_96**)** of n-dodecane combustion containing 96 species has been obtained using the approach previously described by Stagni et al. [7] and Ranzi et al. [19]. This reduced or skeletal kinetic scheme is discussed in the kinetic section of this paper and then used in the section of the spray engine modeling. The Supplemental material reports more details about the reduction procedure, the errors compared with the complete kinetic scheme, and the error maps (Fig. S1 in the SM) in the range of the validation conditions.

**Table 1**
n-dodecane skeletal mechanisms used in this work.

| | Number of species | Number of reactions | Max error (%) | Original mechanism |
|---|---|---|---|---|
| Luo et al. [13] | 105 | 420 | 30 | [27] |
| Narayanaswamy et al. [25] | 255 | 2289 | 18 | [27] |
| Polimi_NC12_96 | 96 | 993 | 15 | [Polimi |
| (extension to PAHs) Wang | (133) | (2275) | | TOT1407] |
| et al. [26] | 100 | 432 | – | [28] |

## 3. Validation of the skeletal model and comparison with similar literature mechanisms

This section contains an extensive validation study of the skeletal Polimi_NC12_96 kinetic mechanism in a very wide range of conditions, together with a similar validation and comparison with other n-dodecane skeletal mechanisms recently proposed in the literature. Table 1 compares the schemes of Narayanaswamy et al. [25], containing 255 species and 2289 reactions, the mechanism of Luo et al. [13] containing 105 species and 420 reactions, and the mechanism of Wang et al. [26] which has 100 species and 432 reactions. All these mechanisms were already validated and developed with accuracy targets similar to the ones adopted in this work. The mechanisms of Luo and Narayanaswmay were obtained from the detailed mechanism of Sarathy et al. [27], while the mechanism of Wang from the previous scheme of Westbrook et al. [28]. Luo et al. [13] adopted a combination of directed relation graph (DRG) [29] with expert knowledge (DRGX) [30] and DRG-aided sensitivity (DRGASA) [31] to obtain their skeletal mechanism. Narayanaswamy et al. [25] reduced the de-tailed scheme of Sarathy et al. [27] to a skeletal level using a multi-stage reduction strategy, involving automatic species and reaction elimination using the DRGEP approach [32], and chemical lumping of species [33]. Wang et al. [26] adopted a similar procedure based on the DRGEP method [32] with reaction pathway and sensitivity analyses to reduce the detailed mechanism of Westbrook et al. [28].

It is first useful to compare the structure of these mechanisms to highlight difference and similarities. Table 2 shows a comparison of the relevant species with 12 carbon atoms, formed in the low temperature oxidation of n-dodecane. The Luo mechanism maintains a small subset of the original isomers contained in the original detailed mechanism [27], while the other schemes also take advantage of the lumping approach to further reduce the number of species. Figure 1 shows the effect of the reduction on the number of species and their distribution in a C–H plane. It is possible to observe that the Luo mechanism only contains heavy species with high H/C ratios, i.e. the reduction phase eliminated all the heavy dehydrogenated and aromatic species. It is also evident that the mechanism still contains a relatively large number of species with 12 carbon atoms. The Wang mechanism has a similar structure, but takes advantage of the lumping approach and therefore it has only 5 species with 12 car-bon atoms. As already observed in Table 2, Narayanaswamy et al.[25] partially used lumping rules to reduce the total number of iso-mers. This mechanism also contains heavy dehydrogenated species and PAHs leading to soot precursors, located in the region of the diagram corresponding to heavy species with low H/C ratios. The Polimi mechanism with 96 species has a similar structure, and thanks to the "horizontal lumping" approach it contains 6 species with 12 carbon atoms. This strategy is also combined to a "vertical lumping": homologous species with 8, 9 and 11 carbon atoms are split between the two closest references (7, 10 or 12) according to the lever rule. Doing so, the total number of stable species is further reduced [6]. By adding a sub-set of 37 species and 1282 reactions, the mechanism can be extended to include benzene, indene, naphthalene, methylnaphthalene, acenaphthylene, phenantrene, biphenyl, fluorene and other aromatics up to $C_{20}$. Similarly, the scheme of Wang includes PAHs up to

**Table 2**
Relevant species with 12 carbon atoms.

| | Alkyl $R^{\bullet}$ | Peroxy $ROO^{\bullet}$ | Hydroperoxy-alkyl •QOOH | Hydroperoxy-alkylperoxy •OOQOOH | Keto-hydroperoxydes | Total |
|---|---|---|---|---|---|---|
| Detailed | 6 | 6 | 30 | 30 | 30 | 102 |
| Narayanaswamy | 1(lumped) | 1(lumped) | 3 | 2 | 2 | 9 |
| Luo | 4 | 3 | 4 | 4 | 5 | 20 |
| Wang | 1(lumped) | 1(lumped) | 1(lumped) | 0 | 1(lumped) | 4 |
| Polimi | 1(lumped) | 1(lumped) | 1(lumped) | 1(lumped) | 1(lumped) | 5 |

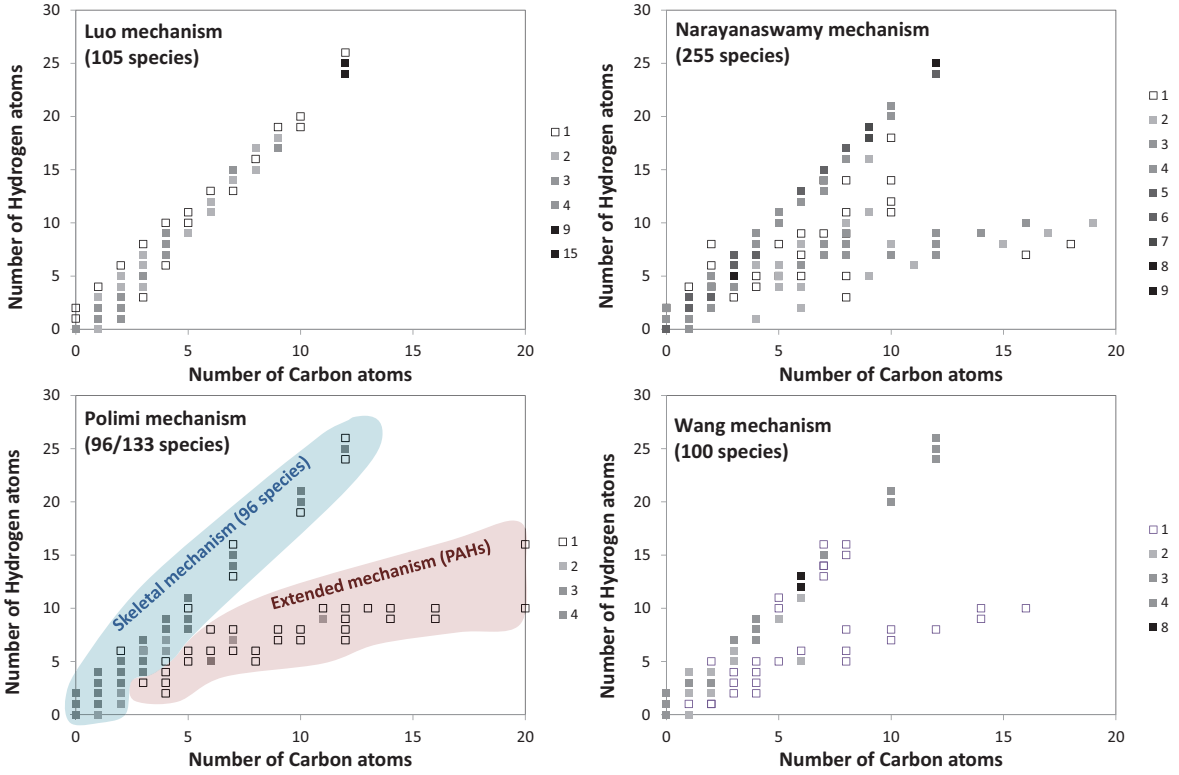


**Fig. 1.** Scatter plots showing the distribution of the species in a C–H plot. The color of the symbols shows the number of species with the same number of Carbon and Hydrogen atoms.

pyrene ($C_{16}H_{10}$) and the mechanism of Narayanaswamy up to A4R5 ($C_{18}H_{10}$).

Table 3 summarizes the whole set of experimental data, including autoignition at very low temperatures and pressures, pyrolysis conditions, and autoignition of isolated fuel droplets in microgravity. All the simulations discussed in this section are performed using the computational tools belonging to the OpenSMOKE++ library [48]. Due to the large number of experimental data and conditions, only a few comparisons will be discussed, while the remaining ones are reported in the Supplemental material (SM).

According to Table 3, the following experimental conditions will be analyzed:

3.1 Ignition delay times and species time history in shock tubes and batch reactors,
3.2 n-dodecane oxidation in Plug Flow Reactors,
3.3 n-dodecane pyrolysis and oxidation in jet stirred reactors,
3.4 laminar flame speed of n-dodecane,
3.5 auto-ignition of isolated droplets in microgravity.

### *3.1. Ignition delay times and species time history in shock tube and batch reactors*

The ignition delay was calculated for several n-dodecane/air mixtures and different pressures. Panels (a) and (b) of Fig. 2 show the comparison with the autoignition experimental data of Vasu et al. [34] at 20 atm. It is possible to observe that the four mechanisms agree rather well with the experimental data and are able to reproduce the NTC phenomena. The NTC effect is more pronounced in the case of the Luo mechanism, while the predictions of the Narayanaswamy, Wang, and Polimi mechanisms are closer to the experimental data. Similar results are also reported in panels (c) and (d) of Fig. 2, which compares model predictions and the autoignition delay times reported by Davidson et al. [37] and Shen et al. [35]. In these conditions, the Wang mechanism tends to over-estimate the reactivity at 6 atm.

Figure 3a compares the ignition delay times with experimental data at ∼2 atm [36]. They are measured referring to the half-peak concentrations of OH. The Narayanaswamy scheme is the least reactive in all the conditions of Fig. 3, while the Wang mechanism is the most reactive. Figure S4 in the Supplemental material contains further comparisons and shows that while the four mechanisms predict similar ignition delays based on OH half-peak, the agreement is different when $C_2H_4$ or $H_2O$ half-peaks are used to define the ignition delays.

Figure 3b shows a comparison with the low temperature autoignition experiments of Wilk et al. [39], who measured the effect of pressure on the induction period of the first cool flame in a batch reactor. (See Fig. S5 in SM for additional comparisons with experimental data

**Table 3**
Summary of the experimental n-dodecane pyrolysis and oxidation data analyzed for kinetic models validation. An additional extensive kinetic validation is reported in the Supplemental material of this paper.

| Operating conditions | Temperature (K) | Pressure (atm) | Equivalence ratio | Reference |
|---|---|---|---|---|
| Ignition delay and species time history in ST | 727–1422 | 15 and 20 | $\Phi = 0.5$, $\Phi = 1.0$ in air | Vasu et al. [34] |
| | 1158–1422 | 16 | $\Phi = 0.5$ (21% $O_2$ in Ar) | Vasu et al. [34] |
| | 786–1396 | 40 | $\Phi = 0.5$ in air | Shen et al. [35] |
| | 1300–1600 | 2 | $\Phi = 1$ (~400 ppm in Ar) | Davidson et al. [36] |
| | 1050–1350 | 6.7 | $\Phi = 0.5$ (21% $O_2$ in Ar) | Davidson et al. [37] |
| | 867–1739 | 23–51 | $\Phi = 1$, $\Phi = 1.06$, $\Phi = 2.05$ | Malewicki&Brezinsky [38] |
| Batch reactor | 523–623 | 0.13–0.53 | $\Phi = 1$ in air | Wilk et al. [39] |
| Plug Flow Reactor (PFR) | 500–1000 | 8 | $\Phi = 1$ (250 ppm in $O_2/N_2$) | Veloo et al. [40] |
| | 550–830 | 8 | $\Phi = 0.23$ (531 ppm in $O_2/N_2$) | Kurman et al [41] |
| Jet Stirred Reactor (JSR) | 550–1150 | 10 | $\Phi = 0.5$, $\Phi = 1$, $\Phi = 2$ (1000 ppm in $O_2/N_2$) | Mzé-Ahmed et al. [42] |
| | 773–1073 | 1 | $\Phi = \infty$ (20,000 ppm in He) (simulated $N_2$) | Herbinet et al [43] Kumar |
| Laminar flame speed | 400–470 | 1 | $\Phi = 0.7$–$1.4$ in air | and Sung [44] |
| | 403 | 1 | $\Phi = 0.7$–$1.5$ in air | Ji et al. [45] |
| | 400 | 1,2,3 | $\Phi = 0.7$–$1.4$ in air | Hui and Sung [46] Tanabe |
| Droplets in microgravity conditions | 600–1000 (ambient $T$) | 1–20. | Fuel droplet in air | et al. [47] |

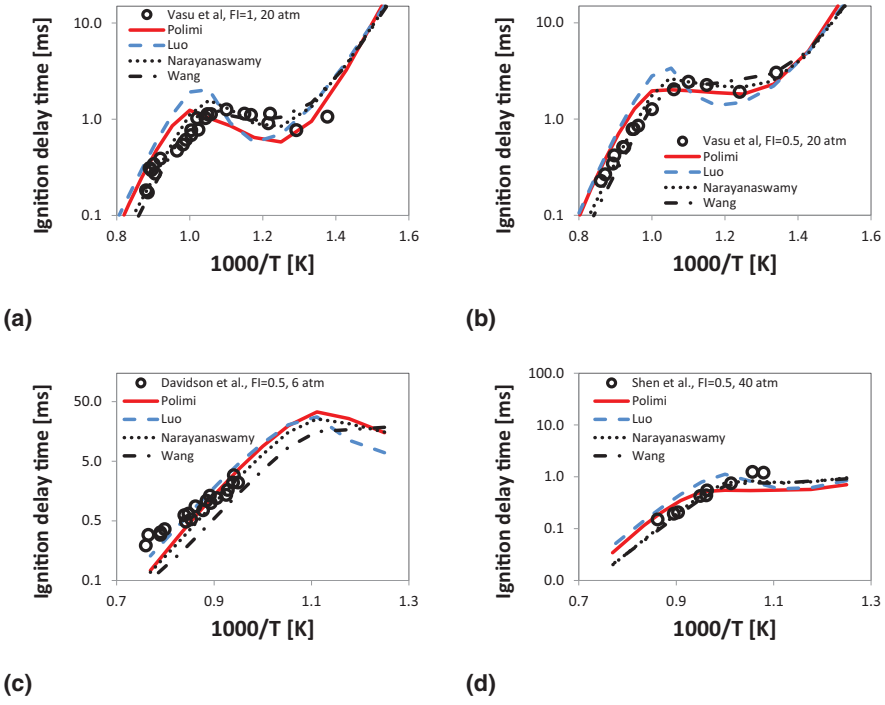


**Fig. 2.** n-Dodecane/air ignition delay times. Panel (a) $\Phi = 1$ and 20 atm [34]. Panel (b) $\Phi = 1$ and 20 atm [34]. Panel (c) $\Phi = 0.5$ and 6.7 atm [37]. Panel (d) $\Phi = 1$ and 40 atm [35]. Comparison of experimental data (symbols) and model predictions (lines).

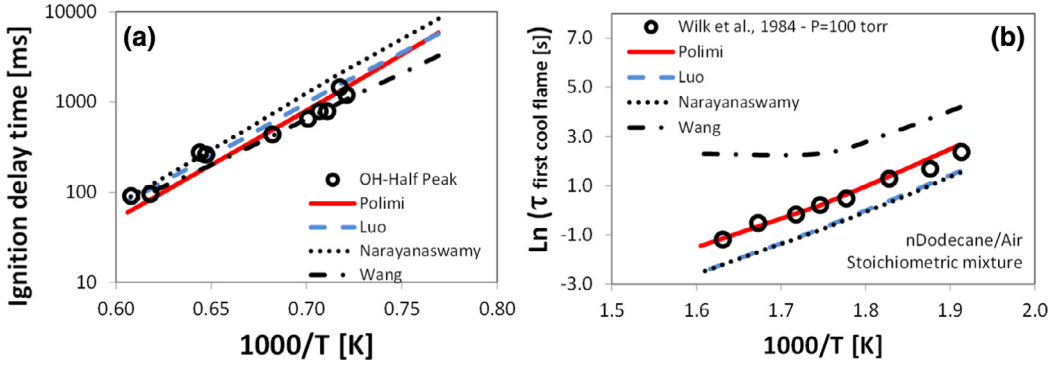


**Fig. 3.** Panel (a) ignition delay time measurements for n-dodecane. Initial conditions: 2.25 atm, 400 ppm of n-dodecane in $O_2$/Ar at $\Phi = 1$ [36]. Ignition delay time defined as the time to half-peak concentration for OH. Panel (b) induction period of the first cool flame of a stoichiometric n-dodecane mixture in air [39]. Symbols represent experiments, lines are predictions of the four kinetic schemes.

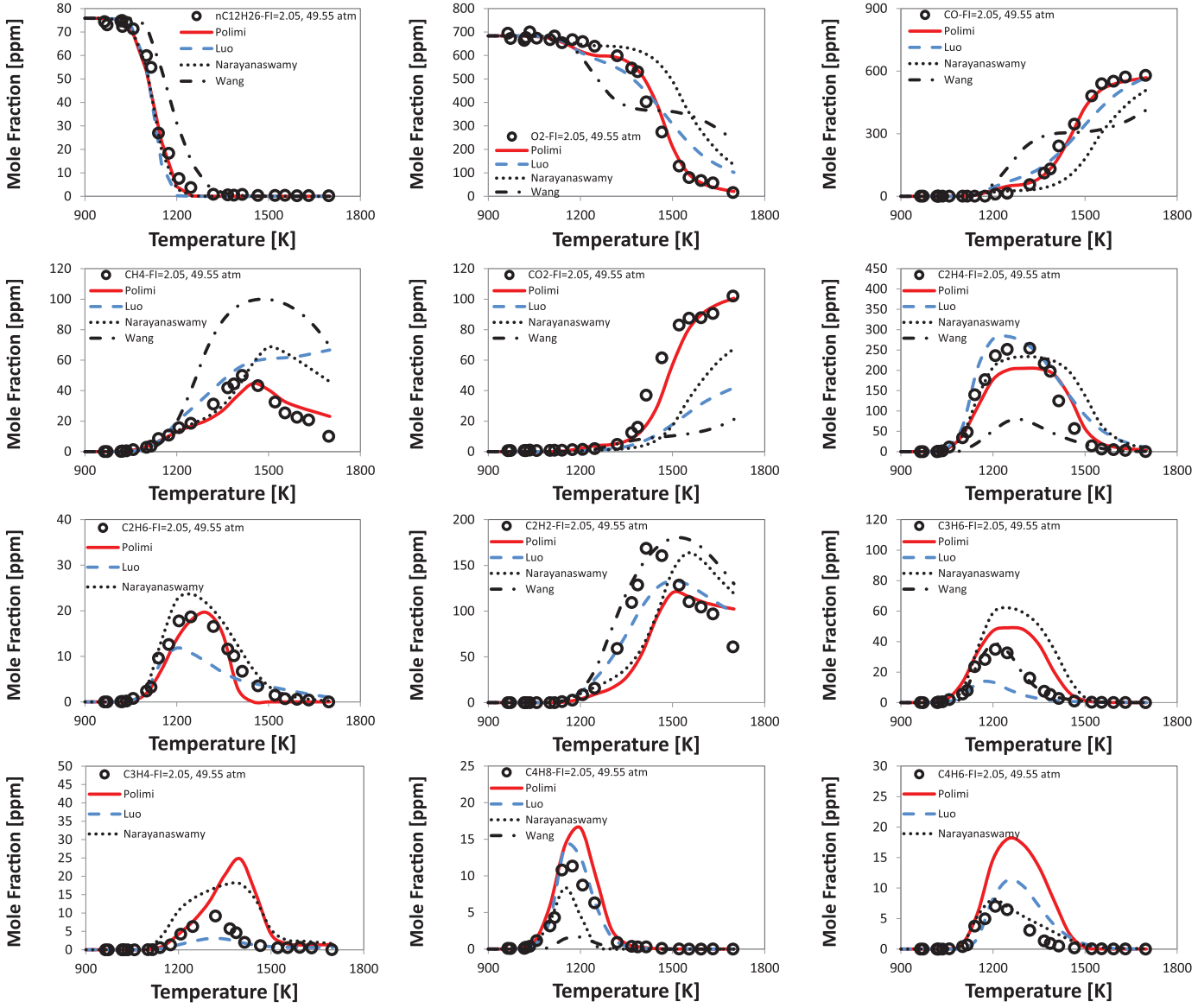


**Fig. 4.** Mole fractions of major species during the oxidation of a n-dodecane/$O_2$/Ar mixtures at $\Phi = 2.05$ $P = 49.55$ atm. Symbols represent experiments from Malewicki and Brezinsky [38], lines are predictions of the different kinetic schemes.

of Wilk et al. [39]). In these conditions, the Polimi mechanism generally well reproduces the ignition time, with Luo and Narayanaswamy showing virtually the same predictions, and the mechanism of Wang, which over-estimates the induction times. This different reactivity at low temperatures will be better discussed in the comparisons with Flow Reactor experiments and autoignition of isolated fuel droplets in the next paragraphs.

Mole fractions of stable species produced during pyrolysis and oxidation of n-dodecane in a shock tube were measured by Malewicki and Brezinsky [38] at high pressures, different temperatures, and a reaction time 1.15–3.47 ms. These times vary with the temperature and they correspond to the 80% of the maximum pressure rise. Computed results were obtained using a constant-volume batch reactor and the simulation time corresponding to the measured reaction time for each simulated condition. Figure 4 (and S6–S10 in the SM) show a detailed comparison between measured and predicted species profiles. With the exception of the Wang mechanism, the fuel consumption profile is well captured by the kinetic schemes in all the conditions. The deviations of Wang mechanism are also confirmed in Fig. S2 in the SM: there is a fast formation of CO at lower temperatures (with the relating consumption of $O_2$) and there is a delayed formation of ethylene and other species formed during the primary decomposition of the fuel. This behavior is particularly evident in rich conditions, and mainly in pyrolysis conditions (Fig. S9 and S10 in the SM). There is also a significant over-prediction of methane, likely due to the removal of ethane from Wang mechanism. Since ethane is not present, methyl radicals cannot recombine, thus favoring the formation of methane. The other three kinetic schemes generally well agree with experimental data in lean conditions for major species, while discrepancies are present for C2–C4 species. The over-estimation of $C_3H_4$ observed for the Polimi mechanism is due to the absence of benzene and larger PAHs in the scheme with 96 species. This deviation disappears if the extended mechanism is adopted, as discussed in paragraph 4. Larger differences are present in stoichiometric and fuel-rich conditions. The Polimi mechanism is the most reactive, while Luo and especially Narayanaswamy show a more pronounced delay in the consumption of $O_2$ and the corresponding formation of CO and $CO_2$. These skeletal mechanisms are able to reasonably reproduce also the pyrolysis data. It is also possible to observe that the Polimi and Narayanaswamy predict very similar

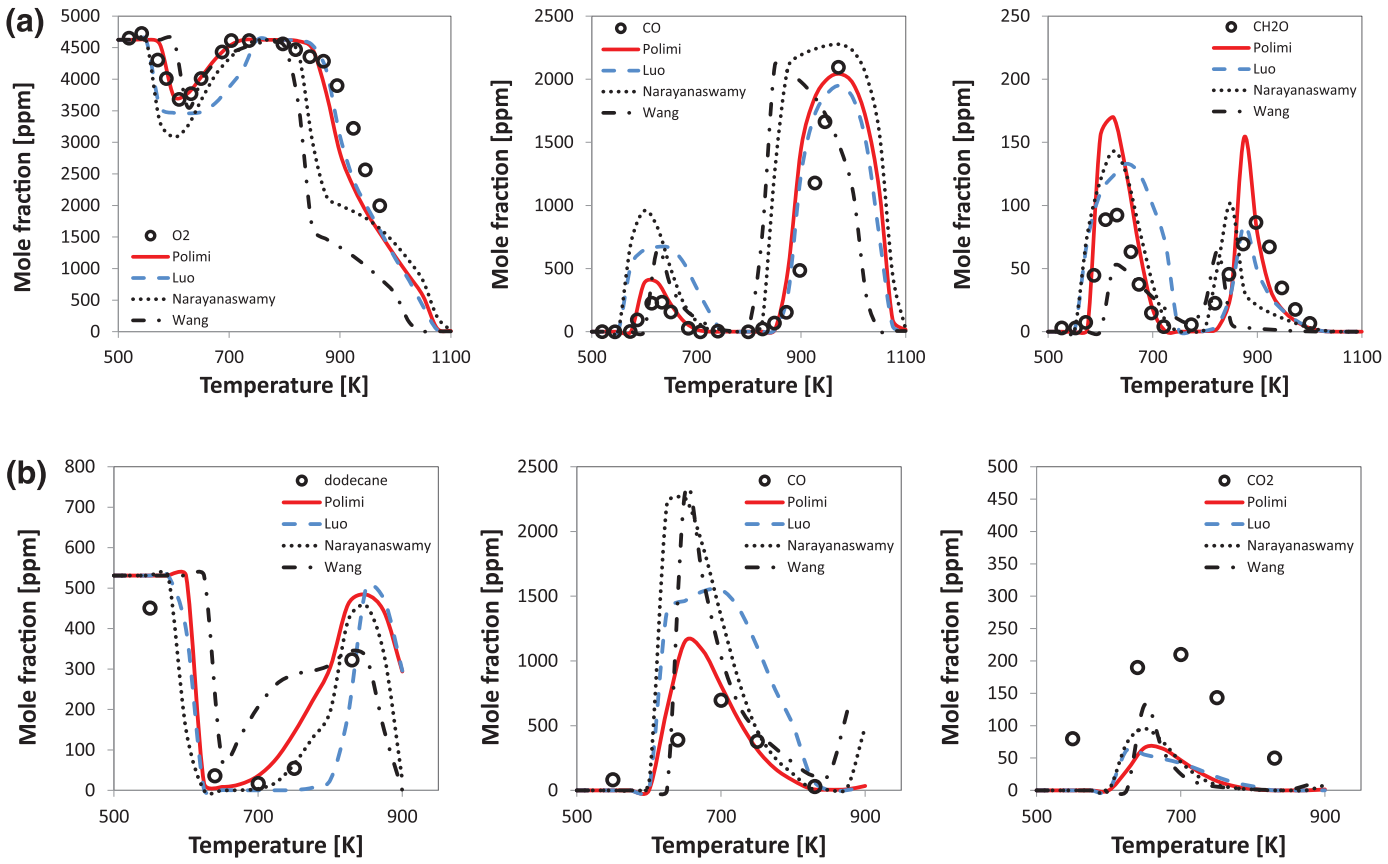


**Fig. 5.** Flow reactor oxidation n-Dodecane/$O_2$/$N_2$ mixtures at 8 atm. Comparison of experimental data (symbols) and predictions of the four skeletal mechanisms. Panel (a) 250 ppm of n-dodecane, $\Phi = 1$ and $\tau = 1$ s (Veloo et al. [40]). Panel (b) 531 ppm of n-dodecane $\Phi = 0.23$ and $\tau = 0.12$ s (Kurman et al. [41]).

ethylene yields while Luo tends to slightly overestimate $C_2H_4$ in pyrolysis conditions.

### 3.2. *n-dodecane oxidation in Plug Flow Reactors*

Figure 5 shows the flow reactor oxidation experiments performed at Princeton [40] and Drexel [41] Universities at 8 atm and different temperatures, covering the low and high temperature regions. The comparison shows that the Polimi mechanism is able to reproduce the low temperature reactivity in the Princeton experiments correctly, while Narayanaswamy and Luo mechanisms show a more pronounced reactivity. The Wang scheme shows a slight delay in the onset of the low temperature region. These deviations at low temperatures are consistent with the ones already observed in the autoignition experiments of Wilk et al. [39], shown in Fig. 3.

It is also interesting to observe that the high temperature reactivity (above ~900 K) is over-estimated by all the mechanisms, by 20–30 K (Luo and Polimi), ~80 K (Narayanaswamy) and ~100 K (Wang). This deviation is not fully consistent with the similar ones of the autoignition shock tube experiments. The onset of the NTC region is well predicted by the Polimi and Wang mechanisms in the Princeton [40], while the Narayanaswamy mechanism better agrees with Drexel data [41]. The Luo mechanism shows an overestimation of the low temperature reactivity, in both experiments.

### 3.3. *n-dodecane pyrolysis and oxidation in jet stirred reactors*

This section compares the predictions of the kinetic schemes with the oxidation and pyrolysis experimental of in JSR at 1 and 10 atm [42,43]. Figure 6 (and S11–S13 in the SM) allows to observe the effect of temperature and equivalence ratio on the oxidation of n-dodecane at 10 atm.

The NTC region is evident in all the conditions and is generally well reproduced by the models. The Luo mechanism well predicts the n-dodecane in lean conditions (Fig. S11 in the SM) but becomes too reactive moving to rich conditions. As already observed in Fig. 5, the Wang mechanism tends to anticipate the hot temperature ignition as evidenced by the CO and $CO_2$ profiles. In these condi-tions, the Polimi model gives an accurate prediction of the profiles of the different aldehydes, especially $CH_2O$ which is under-predicted by the other mechanisms. Acetaldehyde is overestimated by Wang and underestimated by Narayanaswamy. Ethylene is well predicted by Narayanaswamy and Polimi mechanisms, over-predicted using the scheme of Luo especially in lean conditions, and under-predicted by the Wang mechanism as also already observed in the shock tube experiments of Davidson et al. [36] (Fig. S2 in SM) and Malewicki and Brezinsky [38] (Fig. 4 and S6–S10 in SM). A similar deviation is present in the pyrolysis data of Herbinet et al. [43] shown in the SM (Fig. S13). Figure 6 also shows that acetylene is formed in small amounts in these conditions. The Polimi mechanism well agrees with the lean data, especially at low temperatures, while Narayanaswamy and Luo better agree in moderately rich conditions. Only the Polimi and Narayanaswamy mechanisms provide a good prediction of large oxygenated products such as propanal, butanal, and acrolein. The acetylene predictions of Wang mechanism are in excess in pyrolysis and in large defect in oxidation conditions. Polimi tends to overestimate acetylene in the JSR conditions of Fig. 6 (and S11–S13). This deviation is the opposite of the one observed for the Polimi mechanism in Fig. 4 (and Fig. S6–S10 in the SM).

### 3.4. *Laminar flame speed of n-dodecane*

Figure 7 shows a comparison between predicted and experimen-tal laminar flame speeds of n-dodecane/air [44–46], with attention

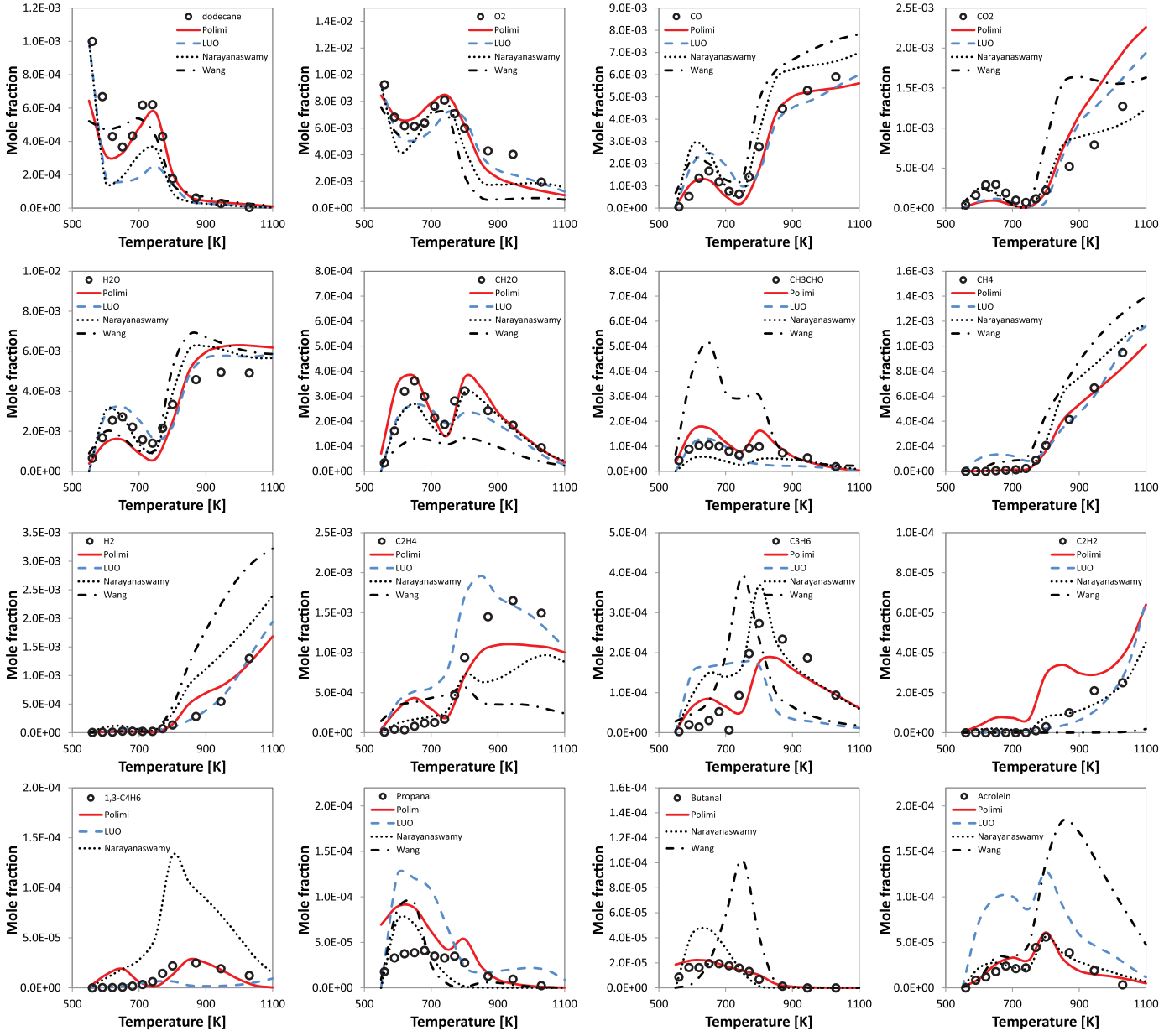


**Fig. 6.** Jet Stirred reactor oxidation n-dodecane/$O_2$/$N_2$ mixtures at 10 atm, $\tau = 1$ s and $\Phi = 2.0$. Comparison of experimental data (symbols) [42] and model predictions (lines).

to the effects of pressure and initial temperatures. The Polimi and Narayanaswamy schemes correctly predict the laminar speeds in the different conditions, while the Luo and Wang mechanisms show significant deviations. The Luo mechanism underpredicts the flame speed of ~10 cm/s, especially in stoichiometric and fuel lean conditions. This deviation has been already discussed by Luo et al. [13] and is associated with the reduction of the kinetic mechanism. On the contrary, the Wang mechanism shows good predictions in lean conditions, but significant over-predictions (up to ~12 cm/s) in rich conditions. The sensitivity analysis presented in Table 4 shows the relevant role of the $C_0$–$C_2$ sub-mechanism, and particularly of the reactions of methyl and vinyl radicals. The major difference among the schemes is associated with the production and consumption routes of $CH_3$ radicals. Beside H-abstraction reactions on $CH_4$,the four mechanisms mainly form $CH_3$ through the $\beta$-decomposition re-action of n–$C_3H_7$ radicals, via $C_2H_5$+H=$CH_3$+$CH_3$ and via the de-composition of s-$C_3H_5$ to $C_2H_2$ and $CH_3$. A relevant role is also played by the reactions $C_2H_4$+O=HCO+$CH_3$ and $O_2$+$C_2H_3$=$CH_2$CHO, which ultimately leads to the formation of $CH_3$ and CO. Relevant differences are present for the consumption routes of $CH_3$ radicals. Polimi and Narayanaswamy consume $CH_3$ via recombination reactions to form $CH_4$ and $C_2H_6$, followed by the oxidation of $CH_3$ via OH or O. The mechanisms of Luo and Wang mainly oxidizes $CH_3$ via $CH_3$+O=$CH_2$O+OH. This channel accounts for about 40% of the total $CH_3$ consumption for the Wang mechanism and 25% for Luo, while the oxidation by OH plays a relatively minor role in both mechanisms (about 8%). The very large role of $CH_3$+O in the mechanism of Wang is likely a consequence of the removal of $CH_3$ self-recombination reaction, which accounts for 17%, 18% and 25% of the total $CH_3$ consumption for Luo, Polimi and Narayanaswamy, respectively. This path is not included in the Wang scheme since ethane is not present. It is important to underline the complex role of the pathways initiated via methyl radical recombination on the reactivity of the system especially in rich conditions. The reaction $CH_3$+$CH_3$+M=$C_2H_6$+M is followed by H-abstractions R+$C_2H_6$⇒$C_2H_5$+RH (R=H, OH), forming ethyl radicals which mainly decompose to $C_2H_4$+H or react via H+$C_2H_5$=$CH_3$+$CH_3$. The net results are the chain-terminating global reactions H+R=>RH or $CH_3$+$CH_3$+R=>$C_2H_4$+H+RH. This explains

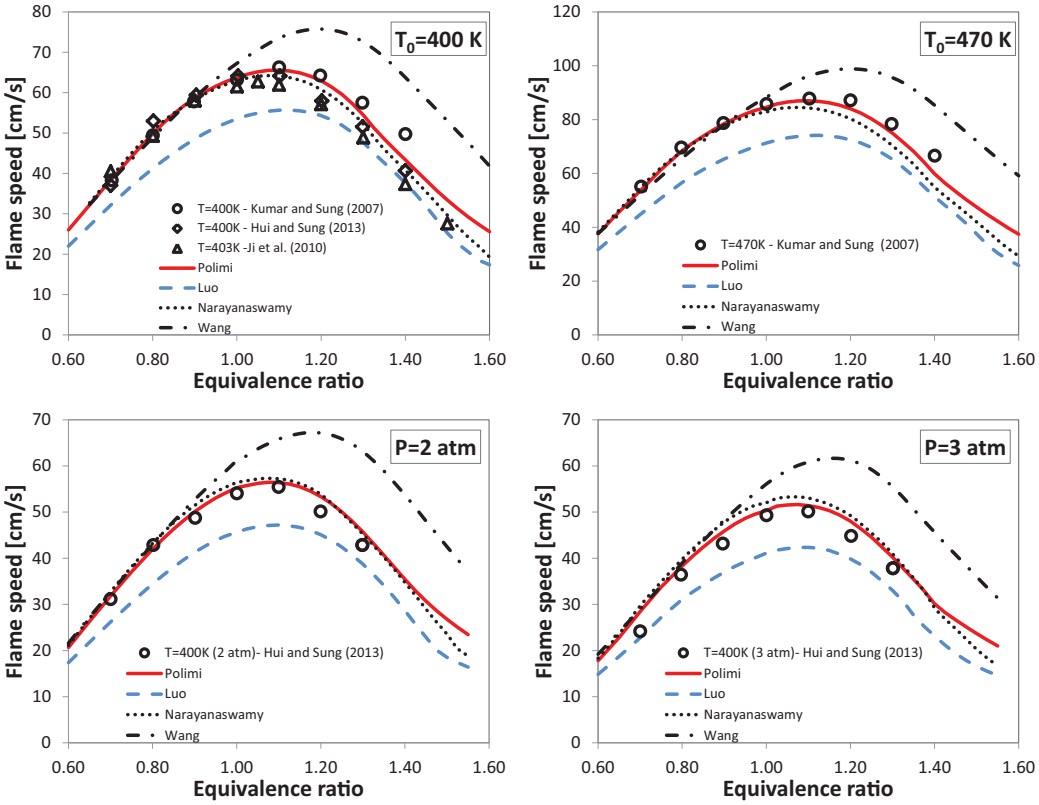


**Fig. 7.** Effect of pressure and initial temperature on the laminar flame speeds of n-dodecane flames in air. Comparison of experimental data (symbols) [44–46] and model predictions.

**Table 4**
Sensitivity analysis for n-dodecane/air flame speed at $T_0 = 400$ K and $\Phi = 1.4$. Ranking of the reaction and corresponding sensitivity coefficient (in parenthesis) for the four mechanisms.

| Reaction/scheme | Polimi | Narayanaswamy | Wang | Luo |
|---|---|---|---|---|
| $H+O_2=OH+O$ | 1 (0.44) | 1 (0.46) | 1 (0.49) | 1 (0.54) |
| $H+CH_3+M=CH_4+M$ | 2 (−0.11) | 4 (−0.062) | 3 (−0.082) | 2 (−0.10) |
| $O_2+C_2H_3=O+CH_2CHO$ | 3 (0.071) | 6 (0.055) | 12 (0.032) | 17 (0.039) |
| $HCO+M=H+CO+M$ | 4 (0.061) | 2 (0.14) | 2 (0.13) | 5 (0.069) |
| $H+C_2H_3=H_2+C_2H_2$ | 5 (−0.045) | 10 (−0.034) | 22 (−0.021) | 4 (−0.087) |
| $H+HCO=H_2+CO$ | 6 (−0.036) | 3 (−0.084) | 5 (−0.066) | 14 (−0.034) |
| | | 5 (−0.062)$AC_3H_5+H=C_3H_6$ | 4 (0.067)$CO+OH=CO_2+H$ | 3 (0.09)$CO+OH=CO_2+H$ |

the very high flame speed predicted in rich conditions and the low amount of ethylene predicted by the Wang mechanism, already observed in Figs. 4 and 6 (and S2,S6–S10 in the SM). On the contrary, the mechanism of Luo tends to form more ethylene, and therefore a lower flame speed is observed. Polimi and Narayanaswmay form almost the same amount of ethylene in the laminar flames in the conditions of Table 4, while Wang forms only 42% of this value and Luo about 160%. The lower tendency to form ethylene of the Wang scheme also ex-plains the relatively low sensitivity of the reactions of vinyl radical observed in Table 4.

A similar comparison with ethylene flame speed measurements (Fig. S14 of the SM) shows deviations similar to those already observed in Fig. 7 for n-dodecane. This suggests that the $C_0$–$C_2$ chemistry is mainly responsible for the failure in predicting the n-dodecane flame speed for the Luo and Wang mechanisms.

### *3.5. Auto-ignition of isolated droplets in microgravity*

In order to further validate the kinetic mechanisms and the importance of the low-temperature chemistry, the auto-ignition of isolateddropletsn-dodecaneinair[47] is analyzed in a wide range of operating conditions, with environment temperatures from 600 K to 1100 K and pressures from 1 bar to 20 bar. The importance of the isolated droplet simulations in the context of spray modeling has been recently discussed Borghesi and Mastorakos [49] from a mixture-fraction perspective for n-heptane. They observed that low-temperature reactions played an important role in the transition of the system from the low temperature ignition to a fully burning state. The mathematical model used to describe the transient evapora-tion, ignition, and combustion of isolated pure fuel droplets in micro-gravity conditions was already discussed in previous works [50,51]. Tanabe et al. [47] experimentally investigated the spontaneous ig-nition of isolated fuel droplets of n-dodecane in microgravity conditions. Suspended fuel droplets (with initial diameter of ∼0.7 mm) were suddenly inserted into a pre-heated furnace in a pressurized chamber. Ignition delay times were measured in a wide range of operating conditions. Ignition regions were mapped on temperature-pressure planes, as reported in Fig. 8. The types of ignition process were specified as no-ignition (NI), cool flame ignition (CF), single-stage (SI) and two-stage (2SI) ignition, similarly to what is reported in premixed gas explosion diagrams. A slow reaction region is present at low temperatures and an explosion region (with the typical hot

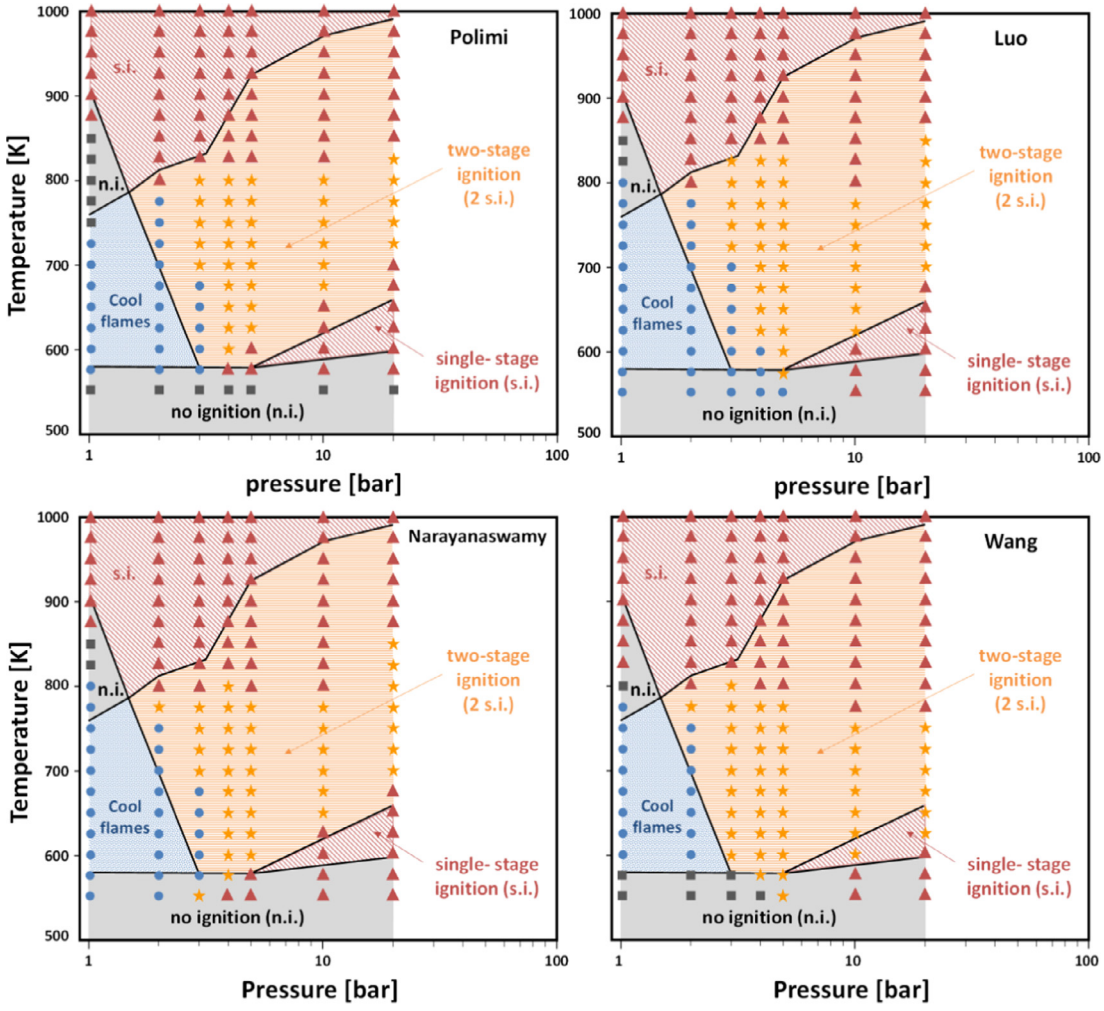


**Fig. 8.** Ignition regions of n-dodecane isolated droplets in air at different pressures and initial temperatures. Comparison between experiments (maps, $d_0 = 0.7$–$0.75$ mm) [47] and numerical predictions (symbols, $d_0 = 0.7$ mm). Grey contour regions and squares: no ignition. Red inclined stripes pattern and triangles: single ignition. Yellow horizontal lines and stars: two-stage ignition. Blue dots pattern and circles: cool flames. (For interpretation of the references to color in this figure legend, the reader is referred to the web version of this article.)

ignition) is found at high temperatures and pressures. The chemistry and the competition between the low- and high-temperature mechanisms are the main reasons of the complexity of such auto-ignition process [51]. In Fig. 8, the symbols represent the results of the numerical simulations and the colored zones were identified by Tanabe et al. [47] on the basis of the experimental measurements.

At low ambient temperatures and all pressures investigated, the droplet vaporizes before chemical reactions lead to autoignition. The Polimi model successfully predicts the region where no ignition occurs at low temperatures (grey zone and square symbols at the bottom of Fig. 8), while both Luo and Narayanaswamy mechanisms are more reactive. A similar deviation, due to a higher reactivity at very low temperatures, has been already observed in the comparison with the autoignition data of Wilk et al. [39] (Fig. 3 and S5) and oxidation in a PFR (Fig. 5). The Wang mechanism is able to accurately predict the boundary of the "no ignition" region, but only at low pressures. The very low reactivity of the Wang scheme at low temperatures and low pressures was already observed in Fig. 3. Narayanaswamy and Luo are very similar at low temperature and pressures, as also observed in Fig. 3, while Narayanaswamy becomes even more reactive moving to higher pressures as also observed in Fig. 5. A similar effect of pressure at low temperatures is also evident for the Wang mechanism.

At low pressures and intermediate temperatures, the low-temperature mechanism becomes effective and the formation of dumped cool flames can be observed. However, in these conditions there is only a limited increase in the temperature and the hot-ignition cannot be reached (blue zone in Fig. 8). The hot-ignition only occurs when the ambient temperature is high enough so that the high-temperature reactions become dominant, but a non-reactive zone is present between cool flames and single ignition. All the kinetic models predicted the "no ignition" zone in the temperature range typical of the NTC region (750–900 K), but the size of this region seems underestimated by the mechanisms of Luo, Narayanaswamy and especially Wang. This deviation is likely associated to the ten-dency of this scheme to anticipate the high temperature ignition and thus reducing the temperature range of the NTC region (see Fig. 5). When the temperature and/or the pressure of the ambient are high enough to make the oxidation reactions competitive with heat trans-fer, a two-stage ignition phenomenon is observed, i.e. a first maxi-mum of temperature, associated to a cool flame, is followed by a hot flame ignition.

## 4. Extended kinetic mechanism (PAHs)

An extended version of the skeletal kinetic model is presented in this section, which allows to predict the formation of cyclopentadiene, methyl-cyclopentadiene, benzene, toluene, phenylacetylene, Indene and naphthalene and larger PAHs up to 20 carbon atoms. These additional species and reactions are also obtained from the original POLIMI_TOT_1407 kinetic mechanism, whose aromatic sub-scheme

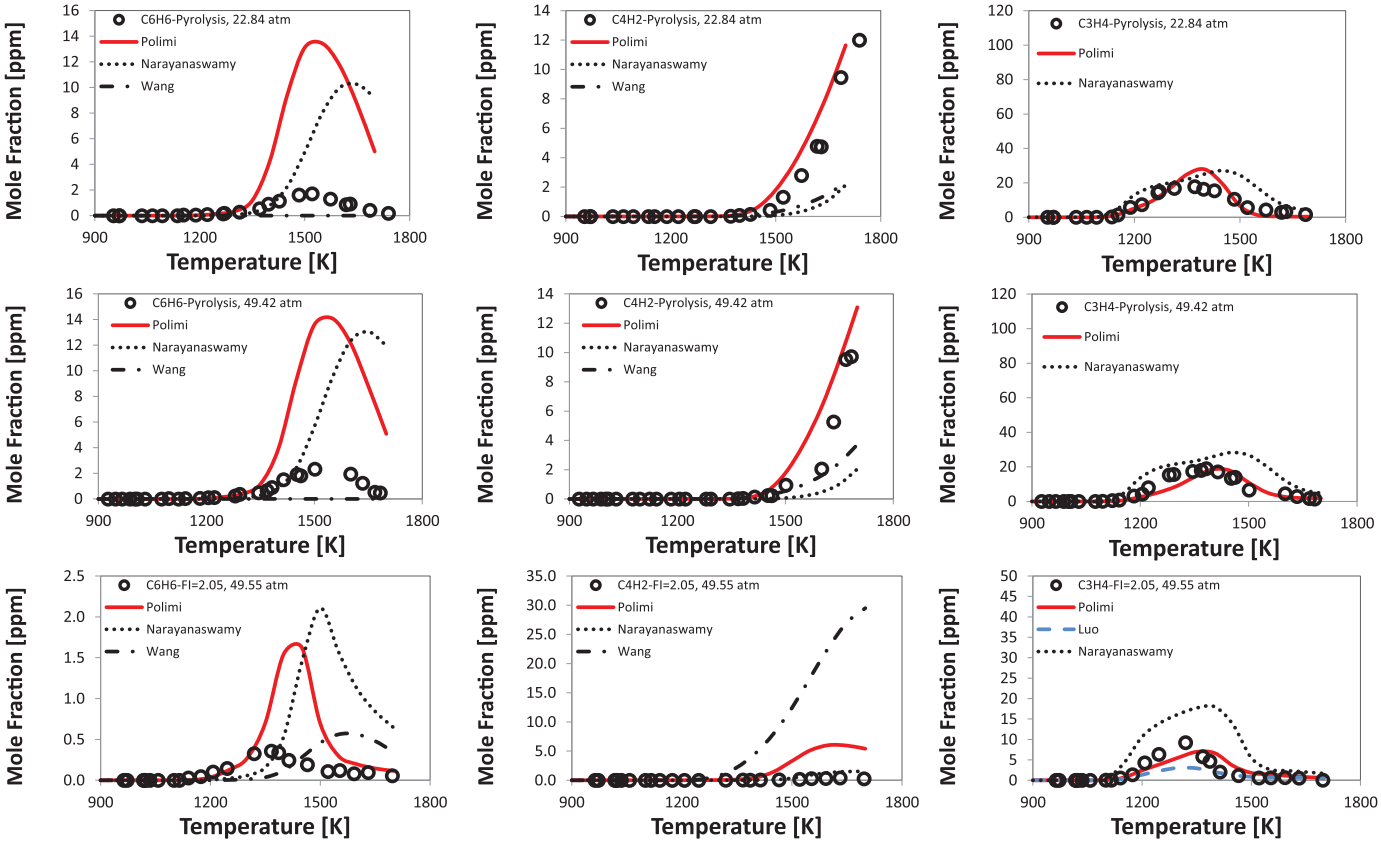


**Fig. 9.** Mole fractions of major species during the pyrolysis and rich oxidation of a n-dodecane/$O_2$/Ar mixtures [38].

has been already discussed in several papers [15,16,18,52,53] and is further extensively validated in the SM.

It is first useful to compare the predictions of this extended model with 133 species with some of the measurements from the experimental datasets already analyzed in the previous paragraphs. Since the reactivity is not significantly influenced by the chemistry of the additional 37 species, ignition delay times and most of the previous results are not presented again in this paragraph. Moreover, the Luo mechanism does not contain any aromatic species and therefore is not used in this section for the comparisons.

Figure 9 shows a comparison with measured values of benzene, $C_3H_4$ and $C_4H_2$ produced during pyrolysis and oxidation of n-dodecane in a shock tube [38], under the conditions already discussed in Fig. 4 (and S9–S10 in the SM). About 1–3 ppm of ben-zene are formed at ~1500 K in the shock tube pyrolysis experiments. Polimi and Narayanaswamy mechanisms overestimate the amount of benzene, but correctly predict the temperature at which the maximum formation occurs and the shift to lower temperatures in the case of rich oxidation. The Wang mechanism predicts almost no benzene formation in pyrolysis conditions, while in oxidation benzene is formed at temperatures about 100–200 K higher than the other mechanisms. The experimental results show that the formation of diacetylene ($C_4H_2$) is quite important in pyrolysis while it is not relevant in rich combustion conditions. The predictions of $C_4H_2$ of the Polimi mechanism well agree with measurements especially in pyrol-ysis while the Wang mechanism shows the opposite deviation. The
over-estimation of $C_3H_4$ observed in Fig. 4 is not present when the extended model is used.

Benzene was also measured by Mzé-Ahmed et al. [42] during the oxidation of n-dodecane in JSR. Detailed comparisons with other species are reported in Fig. 6 (and S11, S12 in the SM). Figure 10 (panels a–c) shows that the Polimi mechanism is able to predict the formation of benzene and the effect of the equivalence ratio in these diluted high pressure and relatively low temperature conditions, while the other mechanism do not form benzene in significant amounts.

To better investigate this point, Fig. 10 also shows a compari-son with the atmospheric n-dodecane pyrolysis experimental data of Herbinet et al. [43]. (This figure completes the comparisons presented in Fig. S13 of the SM with the aromatic species). It is possible to observe that the models of Narayanaswamy and Polimi are generally able to predict the formation of the different aromatic species, although toluene is over-estimated by the Polimi skeletal mechanism. This level of agreement for PAHs is a remarkable result, since these skeletal mechanisms were not obtained to specifically address pyrolysis but mostly oxidation up to moderately rich conditions. The mechanism of Wang also in this case underestimates the formation of benzene, while it predicts a large amount of naphthalene, more than five times larger than benzene.

A more detailed analysis of the formation of PAHs and validation of these mechanisms for the aromatic species is outside the scope of this work and is reported in the SM (Figs. S15–S17).

## 5. CFD simulation of diesel-like spray in constant-volume vessel

The combustion process in diesel-like conditions is here investigated with the four skeletal mechanisms. The so-called Spray-A configuration from the Engine Combustion Network (www.ca.sandia.gov/ecn) was selected for simulation, so that flame structure computed with the different mechanism are examined at different ambient temperatures and oxygen conditions.

### 5.1. CFD numerical methodology

The chosen CFD tool is OpenFOAM®, together with the Lib-ICE set of solvers and libraries developed by the authors to simulate I.C.

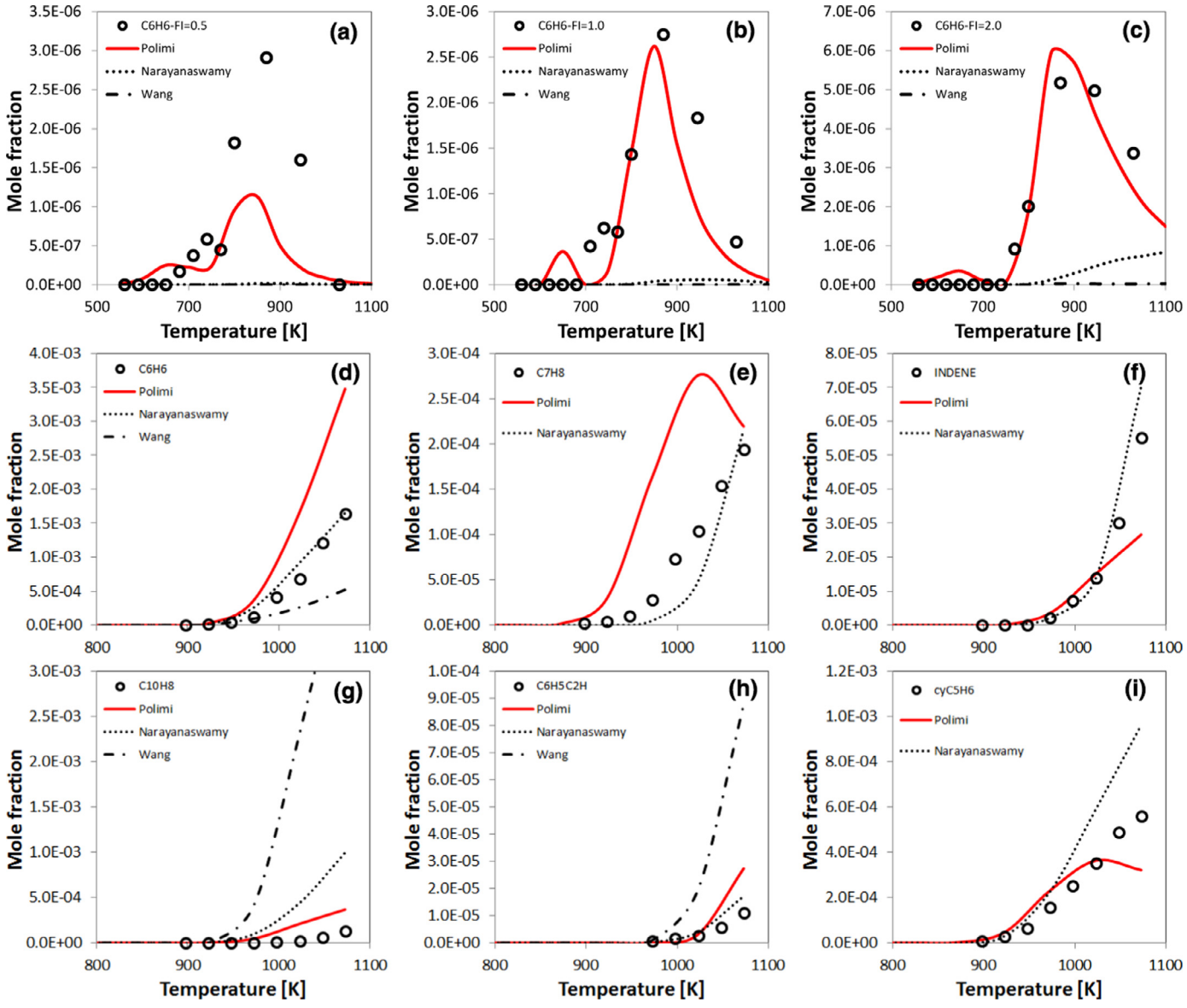


**Fig. 10.** Comparison of experimental data (symbols) and predictions of three n-dodecane skeletal mechanisms. Panels (a–c) Oxidation n-dodecane (1000 ppm)/$O_2$/$N_2$ mixtures at 10 atm, $\tau = 1$ s and different equivalence ratios in a JSR [42]. Panels (d–i) Pyrolysis of n-dodecane/He mixtures at 1 atm and $\tau = 1$ s in a JSR. Comparison of experimental data (symbols) [43] and predictions of the three n-dodecane skeletal mechanisms.

engines [11,54,55]. The gas phase is described using the URANS formulation and mass, momentum and energy equations are solved for a compressible, multi-component flow using the second-order, unstructured finite-volume method supporting polyhedral cells. The $k-\varepsilon$ model was used for modeling the turbulence. Pressure and velocity equations are coupled by the PIMPLE algorithm. The discrete droplet method (DDM) is used to compute the evolution of the liquid fuel spray, which is assumed to be composed by a set of computational parcels, each one of them representative of identical droplets. Parcels are introduced in the CFD domain with the same nozzle diameter. Their initial velocity depends on injected mass flow rate profile and the spray angle is function of nozzle geometry and liquid to gas density ratio [56]. Jet and droplet breakup are computed by the KHRT model, which accounts for both Kelvin–Helmholtz (KH) and Rayleigh–Taylor (RT) instabilities [57]. Concerning other sub-models used, droplet evaporation is computed on the basis of the d-squared law and the Spalding mass number, while the Ranz–Marshall correlation was used to model heat transfer between liquid and gas phases. Collision is neglected since it plays a minor role in evaporating sprays.

The turbulence-chemistry interaction is modeled with the Representative Interactive Flamelet (RIF) model, which couples the solution of the laminar flamelet equations to the solution of the turbulent flow and mixing field. The RIF approach is based on the solution of unsteady laminar flamelet equations for non-premixed systems, with the mixture fraction $Z$ being the independent variable. The local chemical composition in the CFD domain is estimated from the $Z$ field, assuming that its sub-grid distribution can be represented by a $\beta$-pdf. To this end, transport equations for both $Z$ and its variance $\tilde{Z}_{''2}$need to be solved, accounting for the spray evaporation effects [12].

In order to properly account for local flow and turbulence on the flame structure and to predict the flame stabilization, a multiple number of flamelets, $N_f$, is used. Each one is representative of a certain portion of the injected fuel mass. The species mass fraction in each cell $Y_i$ is computed by integrating the flamelet solutions with a

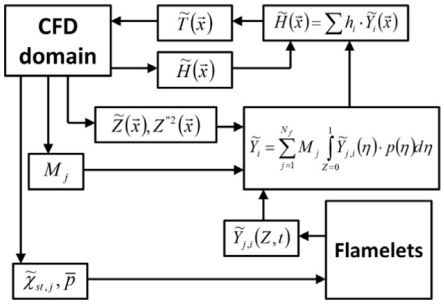


**Fig. 11.** MRIF model: interaction between flamelets and CFD domain.

probability density function $P(Z,\tilde{Z}''^2)$in each CFD cell for all flamelet markers $M_j$:

$$\tilde{Y}_i(\vec{x}) = \sum_{j=1}^{N_f} M_j \int_0^1 \tilde{Y}_{j,i}(Z)\cdot P(Z,\tilde{Z}''^2)dZ \quad (1)$$

In the mixture fraction space the following flamelet equations are solved, assuming unity Lewis number [11,12]:

$$\rho\frac{\partial Y_i}{\partial t} = \rho\frac{\chi_z}{2}\frac{\partial^2 Y_i}{\partial Z^2} + \dot{\omega}_i \quad (2)$$

$$\rho\frac{\partial h_S}{\partial t} = \rho\frac{\chi_z}{2}\frac{\partial^2 h_S}{\partial Z^2} + \dot{q}_S \quad (3)$$

where $Y_i$ is the mass fraction of the species $i$, $\rho$ is the density, $\dot{\omega}_i$ is the chemical source term of species $i$, $h_s$ the sensible enthalpy and $\dot{q}_S$ the heat released by the chemical reactions. Eqs. (2) and (3) are solved on a 1-D mesh with the finite volume method, by employ-ing an ODE stiff solver. Effects of mixing related to turbulence and flow-field are grouped into the scalar dissipation rate term in mix-ture fraction $\chi_z$which is modeled using an erfc-profile and the scalar dissipation rate at stoichiometric mixture fraction for each flamelet computed as an average of the local values in each computational cell [11,12].

Figure 11 summarizes the operation of the MRIF (Multiple Rep-resentative Interactive Flamelets) combustion model, illustrating the mutual interactions between the CFD and flamelets domains. At each time-step, average stoichiometric scalar dissipation rate values are passed to each flamelet, which solves Eqs. 2 and 3 accordingly. The chemical composition in the CFD domain is computed from the mixture fraction, its variance, and the flamelet marker distribution. Temperature is updated from new chemical composition and total enthalpy, whose variation is only due to flow and spray evaporation. For further information, the reader is referred to [11,55,56].

When detailed chemistry is incorporated in CFD combustion mod-els, it is necessary to consider that chemical time-scales are much smaller (2–4 orders of magnitude) than the CFD time-step that is gen-erally used ($10^{-7}$–$10^{-5}$ s). For this reason, ODE stiff solvers need to be employed to properly compute the chemical species reaction rates that are used in the chemical species transport equations. However, stiff ODE solvers significantly increase the computational time since they involve subcycling and computations of large Jacobian matrices. To make the use of relatively detailed mechanisms possible (up to 100 or even 200 species) in a reasonable computational time, the TDAC al-gorithm [11,55] was employed in this work, combining the ISAT and DAC techniques. The ISAT algorithm intends to reuse computationally demanding results, e.g. the integration of large and stiff ODE systems, by storing those results and all the necessary data to retrieve them. The DAC method computes reduced mechanisms that are valid for the local thermo-chemical conditions. In this work, DAC has been ex-tended to full CFD meshes with wall heat transfer. The reduction algo-rithm is executed before every call to the stiff solver according to the directed relation graph (DRG) method, which identifies the relevant species and reactions according to the thermodynamic conditions in each cell [11,55].

Other combustion models with varying degrees of complexity, such as the Unsteady Flamelet Progress Variable (UFPV) [58], the Flamelet Generated Manifold (FGM) [59], the Conditional Moment Closure (CMC) [60,61] and the Transported Probability Density Func-tion (TPDF) methods [62,63], could be used to describe these diesel-like conditions together with the proposed skeletal kinetic model. However the implications due to the employed combustion model are considered to be out of the scopes of the present paper and the reader is referred to the proceedings of the Flame Structure Session of the Engine Combustion Network [64] where such comparisons are performed for the set of experiments described in the following section.

### *5.2. Application to constant-volume spray combustion experiments*

Experiments carried out in a constant-volume vessel and pub-licly available through the Engine Combustion Network were used for validation under diesel-like conditions. The so-called Spray-A configuration was selected for simulation, in which n-dodecane is used as fuel. One operating condition was chosen as baseline, which was intended to represent a low-temperature combustion regime for modern engines [66]. Specifically, it represents a low-temperature, lower-effective-compression-ratio combustion using EGR and intake pressure boost (n-dodecane as fuel, ambient gas initial conditions: temperature 900 K, pressure 60 bar, density 22.8 kg/m$^3$, oxygen concentration 15%). Hence, parametric variations of the operating conditions (ambient temperature and oxygen concentration, fuel pressure) were defined and tested experimentally. Pressure-based ignition delays were recorded together with flame lift-off measure-ments obtained by OH chemiluminescence. Numerically ignition de-lay was defined as the time elapsed from the start of injection to the instant when the rate of rise of the peak temperature is max-imum, as suggested in the Engine Combustion Network guidelines [65]. The influence of ambient temperature and oxygen concentra-tion was assessed in this study, considering four different temper-atures (800 K, 900 K, 1000 K, 1100 K) at constant oxygen concen-tration (15%) and three different oxygen concentrations (13%, 15%, 21%) at constant temperature (900 K), always with a constant den-sity (22.8 kg/m$^3$). Non reacting conditions were first simulated, to properly assess the spray sub-models. Simulations were carried out in a 2D, axy-symmetric mesh with grading (minimum mesh size of 0.1 mm and a successive growth ratio of 1.01). The grid represents a 1/72 portion of the combustion chamber, with a 108 mm height and 54 mm width; it has 216 cells in the axial direction and 108 in the radial one. Concerning the setup of the $k-\varepsilon$ turbulence model, the $C_1$ constant was modified to 1.55 as it is commonly done to predict penetration and diffusion of jets. Validation of the spray model is il-lustrated in Fig. 12a and b for the non-reacting condition ($T = 900$ K, $\rho = 22.8$ kg/m$^3$).

Figure 12a compares computed and experimental data of liq-uid and vapor penetration for different instants after start of injec-tion (ASOI). In Fig. 12b, computed distribution of mixture fraction is compared with post-processed and averaged experimental data that were obtained by means of the Raleigh-scattering technique [65]. The model properly reproduces the experimental trends in terms of liquid and vapor penetration. Furthermore, distribution of mixture fraction is rather well predicted in the entire domain and this is a very impor-tant pre-requisite for the validation of any combustion model.

Once the spray model was properly assessed, combustion simu-lations were carried out. For what concerns the MRIF setup, every 0.1 ms from the start of injection a new flamelet was introduced and initialized with the solution taken from the previous one (both in terms of temperature and chemical species distribution) in the

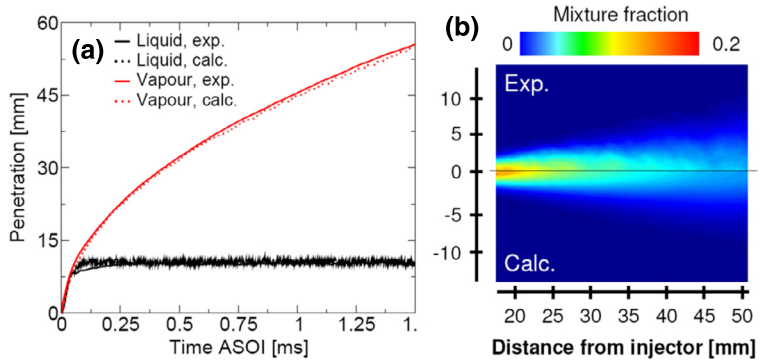


**Fig. 12.** (a) Spray model assessment and validation: comparison between computed and experimental data of fuel liquid and vapor penetrations; (b) comparison between computed and experimental [66] distributions on a symmetry plane at 4 ms after start of injection. Ambient conditions: $\rho = 22.8$ kg/m$^3$; $T = 900$ K.

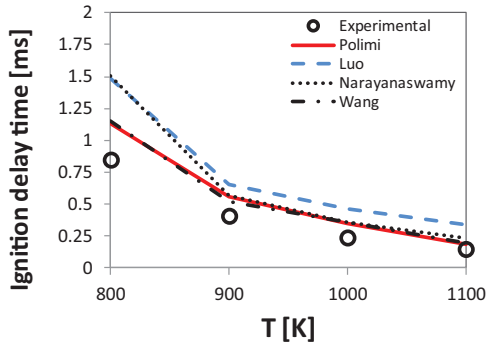


**Fig. 13.** Comparison between measured and computed ignition delay as function of the ambient temperature at constant density (22.8 kg/m$^3$) and constant oxygen concentration (15%).

mixture fraction domain, for all operating conditions apart from the one with an ambient temperature equal to 1100 K. In this case, because of the expected higher reactivity of the mixture, the time interval between two flamelets was reduced to 0.08 ms.

Figure 13 shows the effect of the ambient temperature on ignition delays calculated using the four skeletal kinetic mechanisms of Table 1. The overall trend is captured by all mechanisms, even if results tend to overestimate the onset of high temperature reactions with respect to the experiments. The results obtained using the Polimi and Wang mechanisms are closer to the experimental data for all conditions. The Narayanaswamy mechanism predicts ignition delay times very similar to the predictions of Polimi and Wang mechanisms, apart from the lower temperature condition at 800 K where the ignition delay is significantly overestimated. Among the four mechanisms, Luo shows a higher overestimation of the ignition delay for all conditions.

A comparison of the performance of these kinetic mechanisms under these diesel-like conditions with the previous kinetic analysis carried out in shock tube, plug flow, jet stirred reactors and laminar flames is not trivial. Here we are in presence of fully unsteady flows, typical of evaporating liquid sprays at high temperatures and pressures. Main ignition is mainly caused by the strong reactivity of the rich mixture, diffusing heat and radicals towards the stoichiometric and lean parts of the flamelets. Hence, a proper prediction of the species conversion rate for an equivalence ratio around 2 in the 800–1200 K temperature range at high pressure is crucial. Unfortunately these conditions have not been reproduced in shock tube experiments yet. To better investigate this point a comparison of predicted ignition delay times of the four kinetic schemes at high pressure and rich mixture is presented in Fig. S19 of the SM. In these conditions, the Luo mechanism predicts the longer ignition delays in the whole range of temperature conditions. The Narayanaswamy mechanism gives predictions similar to the Luo mechanism in the low temperature range and to the Wang mechanism at high temperature. The Polimi mechanism is the most reactive in the intermediate temperature range. This observed behavior is fully consistent with the results of ignition delay times presented in Fig. 13. To investigate the influence of the kinetic mechanisms on the flame structure, Fig. 14 shows the computed temperature, OH and $CH_2O$ mass fraction for

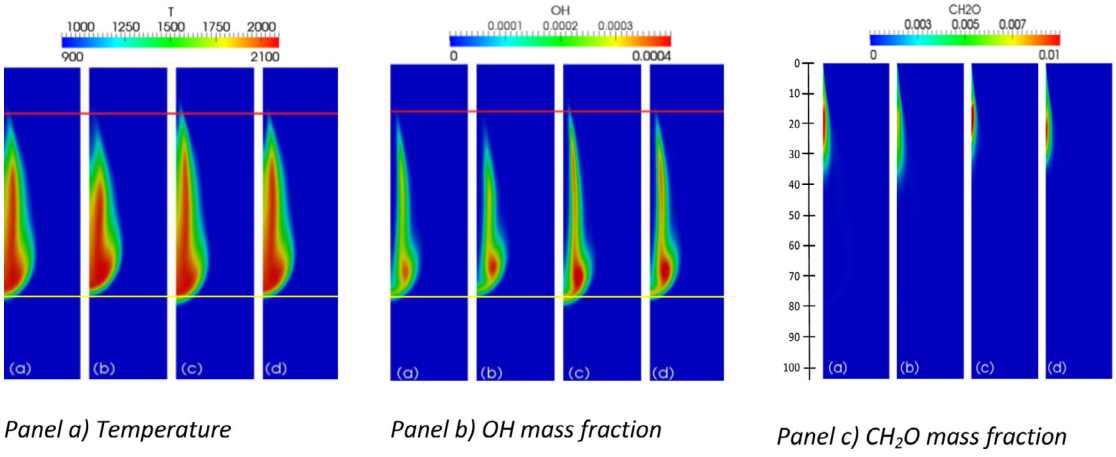


**Fig. 14.** Spray A baseline condition ($T = 900$ K, rho = 22.8 kg/m$^3$, $X_{O2} = 0.15$) at 2.5 ms. Red line: measured lift-off length, yellow line: measured reactive spray penetration [65,66]. Comparison among predicted distributions of temperature, OH and $CH_2O$. Chemical mechanism: (a) Polimi, (b) Luo, (c) Narayanaswamy, and (d) Wang. (For interpretation of the references to color in this figure legend, the reader is referred to the web version of this article.)

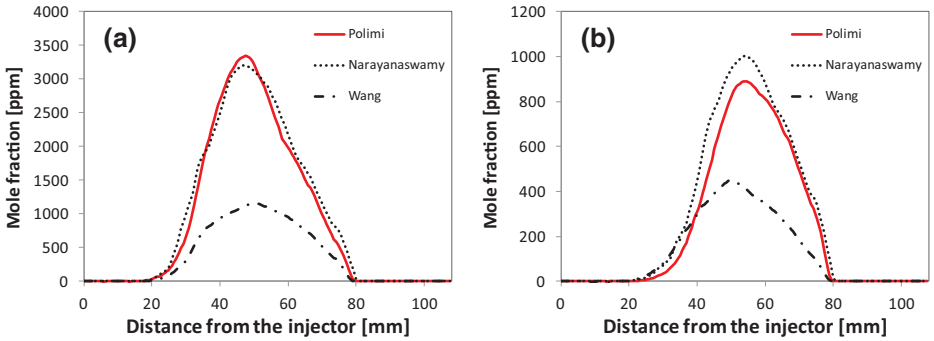


**Fig. 15.** Comparison between computed $C_6H_6$ (a) and $C_{10}H_8$ (b) with the different chemical mechanisms for the Spray A baseline condition ($T = 900$ K, rho $= 22.8$ kg/m$^3$, $X_{O2} = 0.15$) at 2.5 ms along the injector axis.

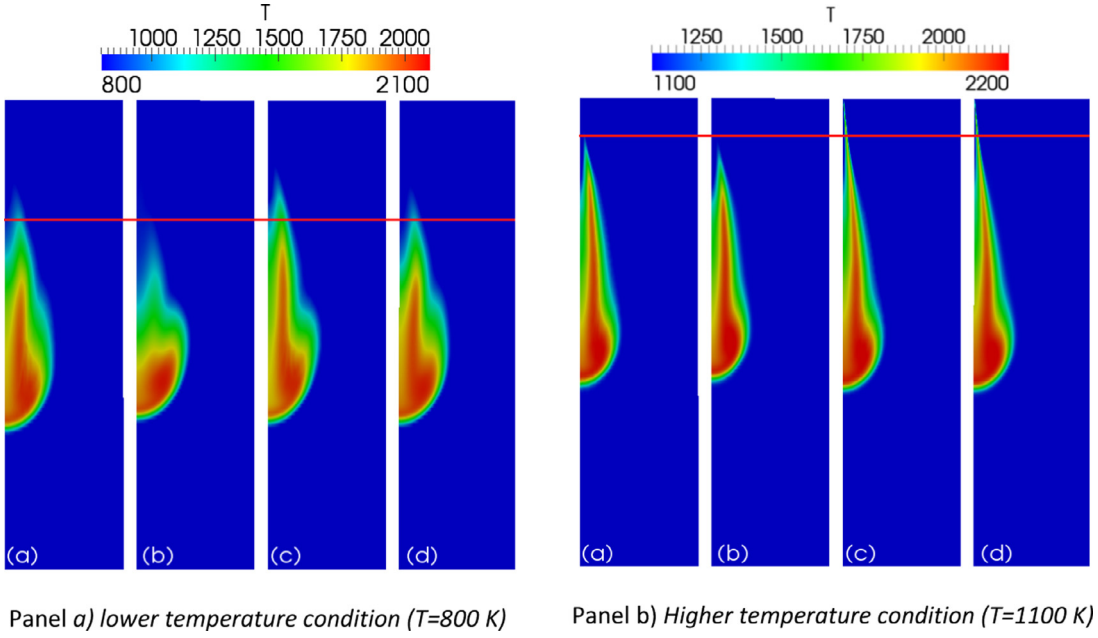


**Fig. 16.** Comparison between computed temperature distributions for the Spray A (rho $= 22.8$ kg/m$^3$, $X_{O2} = 0.15$) at 2.5 ms) at different ambient temperatures. Red line: measured lift-off length [65,66]. Chemical mechanism: (a) Polimi, (b) Luo, (c) Narayanaswamy, and (d) Wang. (For interpretation of the references to color in this figure legend, the reader is referred to the web version of this article.)

the baseline case. In these figures the measured lift-off length and reactive spray penetration are indicated respectively by a red and a yellow line, showing a good prediction of the flame position.

Some differences arise in the temperature and species profile, but the overall flame structure is not significantly influenced by the adopted chemical mechanism and it is not possible to make a quantitative comparison on the basis of the available optical measurements. In the used MRIF combustion model the flame propagation is increased by heat diffusion from the most reactive mixture sites, being the scalar dissipation rate a measure of the mixture fraction gradients and molecular fluxes of the species towards the flame. Hence, the lift-off position occurs where the flame is extinguished by large strain rates and the scalar dissipation rate exceeds the extinction limit. This obviously depends on the chemical mechanism, but also on the local flow characteristics. In general, differences are not remarkable for this condition with respect to the flame lift-off. Only some differences, especially in the predicted absolute values of formaldehyde, can be appreciated, with the Luo mechanism giving the lower values of $CH_2O$ mass fraction. These differences are not the same observed in the case of the (diluted) JSR experiments of Fig. 6. The location of the maximum of formaldehyde is around 20 mm and this is in agreement with the performed PLIF measurements described in [65], whose experimental investigation observed also formaldehyde within few millimeters of the injector tip indicating that low-temperature reactions occur even closer to the injector relative to the lift-off [65]. Figure 15 illustrates the axial profiles of benzene and naphthalene predicted by three kinetic mechanisms. It is possible to observe that the Polimi and Narayanaswmay mechanisms predict almost the same amount of the two aromatic species, while the mechanism of Wang predicts a significantly lower formation of such species. This ten-dency is consistent with the deviations already observed in Figs. 9 and 10, where the Wang mechanism under-predicted benzene thus favoring naphthalene and phenyl-acetylene.

Figure 16 shows the temperature profiles computed respectively for the lower temperature (800 K) and higher temperature (1100 K) case. The models are able to capture the observed Lift-Off Length (LOL) trend with temperature, but a quantitative assessment depends on how the lift-off length is defined. In the ECN network, the LOL was experimentally determined using a threshold of 50% of the chemi-luminescence leveling-off value, while numerically it was defined as the distance from the injector where the OH mass fraction reaches 2% of the maximum in the domain. However, the threshold definition is matter of discussion (other authors [13,62] use a threshold of 14%) and in this paper no quantitative assessment will be given, in order not to drive to some conclusions which basically could depend on a not well stated parameter.

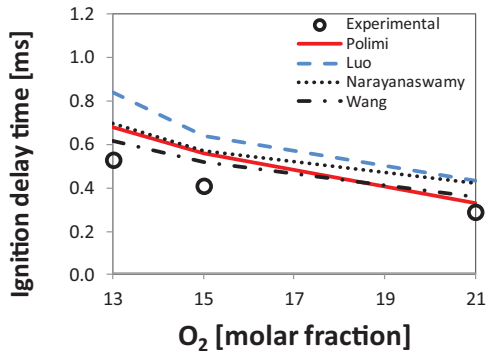


**Fig. 17.** Comparison between measured and computed ignition delay as function of the ambient oxygen concentration at constant density (22.8 kg/m$^3$) and temperature (900 K).

A further analysis of Fig. 16 evidences the differences in the computed flame structure at lower temperature when the Luo mechanism is used with respect to the others. This is due to a less intense low temperature reactivity, consistent with the lower $CH_2O$ level in the zone close to the injector already observed in Fig. 14 for similar conditions. In Fig. 16 , instead, we can observe that the flame is not clearly lifted at higher temperature when the Narayanaswamy and Wang mechanism are used. This difference is fully consistent with the fast ignition observed at temperatures higher than 1000 K in Fig. 2 (and S19 in SM) for the Wang and Narayanaswamy mechanisms, where Polimi and especially Luo mechanisms predict a longer delay time before ignition.

Figure 17 shows the effect of different oxygen concentrations on the ignition delay times. The differences between the kinetic mechanisms are similar those observed in Fig. 13. The overall trend is captured by all mechanisms, even if computed results tend to overestimate the onset of high temperature reactions with respect to the experiments, especially when the Luo mechanism is used. In the lower oxygen concentration case, results obtained using Wang mechanisms are closer to the experimental data, Polimi and Narayanaswamy mechanism predicts very similar ignition delay (with an overestimation of 0.15 ms), while Luo shows a higher overestimation (0.3 ms). In the higher oxygen concentration case, Polimi and Wang prediction are very close to the experimental data, while Narayanaswamy and Luo have a noticeable overestimation.

Finally, Fig. 18 shows the temperature profiles computed respectively for the lower ($X_{O2} = 0.13$) and higher ($X_{O2} = 0.21$) oxygen concentration cases. Also with respect to the ambient condition change, the model is able to capture the observed lift-off length trend with all chemical mechanisms which were tested. When simulating the case with 13% ambient oxygen concentration Luo predicts a less extended high temperature region in the axial direction than the other mechanisms, while the flame structure in the temperature distribution is very similar between Polimi and Wang runs. Similar considerations could be applied to the case with higher oxygen concentration (see Fig. 18 b), even if here differences between Luo and other cases are less remarked.

## 6. Conclusions

The complete POLIMI_TOT_1407 kinetic mechanism has been used for generating a reduced skeletal mechanism, able to represent the combustion properties of n-dodecane in a whole range of conditions. This skeletal model involves 96 species and was obtained using an automatic reduction technique based on reaction flux and sensitivity analyses. The proposed mechanism was extensively validated with available ignition delay times, species concentration profile data from flow reactors and JSRs, and laminar flame speeds. The agreement between experiments and simulations is quite satisfactory. Moreover, the model was further validated using autoignition measurements for n-dodecane droplets in microgravity conditions. An extended version of the Polimi scheme allows the prediction of PAHs up to C20, by adding a subset of additional 37 species.

This skeletal mechanism was compared with two similar skeletal mechanisms from the literature (involving about 100 species) and a larger mechanism with about 250 species. Despite their limited size, these reduced mechanisms were able to accurately describe the high and low-temperature reactivity of n-dodecane in a wide range of conditions. Generally, the Polimi and Narayanaswamy mechanisms gave the best agreement with experimental results, while the Luo

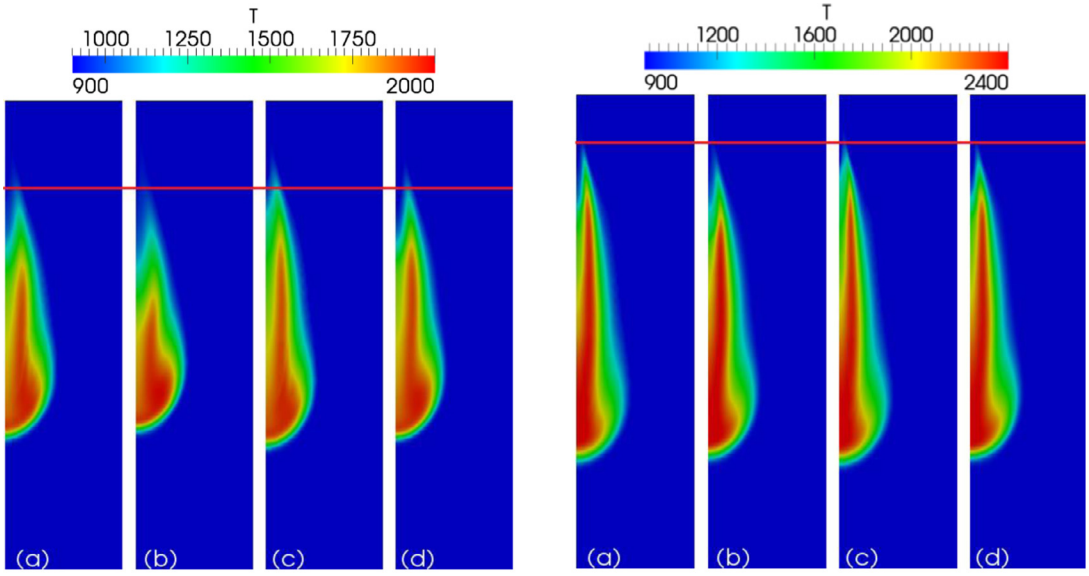


Panel a) *Lower oxygen concentration ($X_{O2}$ = 0.13)*

Panel b) *Higher oxygen concentration ($X_{O2}$ = 0.21)*

**Fig. 18.** Comparison between computed temperature distributions for the Spray A ($T = 900$ K, rho $= 22.8$ kg/m$^3$, at 2.5 ms). Red line: measured lift-off length [65,66]. Chemical mechanism: (a) Polimi, (b) Luo, (c) Narayanaswamy, and (d) Wang. (For interpretation of the references to color in this figure legend, the reader is referred to the web version of this article.)

and Wang mechanisms showed good predictive capabilities, but also some relevant deviations in predicting the low and high temperature reactivity in some conditions (especially the formation of important combustion intermediates and pollutants and the prediction of flame speeds).

These mechanisms were subsequently used in CFD simulations of diesel spray combustion experiments in a constant volume vessel via the development and application of a multiple unsteady flamelet approach. The comparison with the available experiments from the ECN database gave encouraging results in terms of ignition delay and flame liftoff prediction for different ambient temperature and oxygen concentrations, with a tendency to slightly overestimate the ignition delay. The Polimi and Wang mechanisms showed the best predictive capabilities, while the Luo mechanism consistently overestimated the ignition delay in these conditions. The Narayanaswamy mechanism well agreed with experimental measurements and the predictions of Polimi and Wang, but only at high temperatures. This analysis showed that the ignition of rich mixtures and high pressure conditions is critical for the engine simulation and that the validation of the kinetic mechanisms would benefit from new experimental measurements obtained in shock tube reactors in these conditions. The present work supports the use of the present Polimi n-dodecane mechanism for CFD engine simulation, which is obliviously not limited to the MRIF approach used here, and also the generation of an analogous scheme for diesel fuel surrogates.

## Supplementary materials

Supplementary material associated with this article can be found, in the online version.

## References


[1] W.J. Pitz, C.J. Mueller, Recent progress in the development of diesel surrogate fuels, Prog. Energ. Combust. Sci. 37 (2011) 330–350.

[2] F. Battin-Leclerc, E. Blurock, R. Bounaceur, R. Fournet, P.-A. Glaude, O. Herbinet, B. Sirjean, V. Warth, Towards cleaner combustion engines through groundbreak-ing detailed chemical kinetic models, Chem. Soc. Rev. 40 (2011) 4762–4782.

[3] F.L. Dryer, Chemical kinetic and combustion characteristics of transportation fuels, Proc. Combust. Inst. 35 (2015) 117–144.

[4] A. Violi, S. Yan, E.G. Eddings, A.F. Sarofim, S. Granata, T. Faravelli, E. Ranzi, Experimental formulation and kinetic model for jp-8 surrogate mixtures, Combust. Sci. Technol. 174 (2002) 399–417.

[5] S. Dooley, S.H. Won, J. Heyne, T.I. Farouk, Y. Ju, F.L. Dryer, K. Kumar, X. Hui, C.-
J. Sung, H. Wang, The experimental evaluation of a methodology for surrogate fuel formulation to emulate gas phase combustion kinetic phenomena, Comb. Flame 159 (4) (2012) 1444–1466.

[6] E. Ranzi, A. Frassoldati, S. Granata, T. Faravelli, Wide-range kinetic modeling study of the pyrolysis, partial oxidation, and combustion of heavy n-alkanes, Ind. Eng. Chem. Res. 44 (2005) 5170–5183.

[7] A. Stagni, A. Cuoci, A. Frassoldati, T. Faravelli, E. Ranzi, Lumping and reduction of detailed kinetic schemes: an effective coupling, Ind. Eng. Chem. Res. 53 (2014) 9004–9016.

[8] Y. Pei, E.R. Hawkes, S. Kook, A comprehensive study of effects of mixing and chemical kinetic models on predictions of n-heptane jet ignitions with the pdf method, Flow, Turbul. Combust. 91 (2) (2013) 249–280.

[9] J. Tillou, J.-B. Michel, C. Angelberger, D. Veynante, Assessing LES models based on tabulated chemistry for the simulation of diesel spray combustion, Combust. Flame 161 (2) (2014) 525–540.

[10] Y.M. Wright, G. De Paola, K. Boulouchos, E. Mastorakos, Simulations of spray autoignition and flame establishment with two-dimensional CMC, Combust. Flame 143 (4) (2005) 402–419.

[11] G. D'Errico, T. Lucchini, F. Contino, M. Jangi, X.-S. Bai, Comparison of well-mixed and multiple representative interactive flamelet approaches for diesel spray com-bustion modeling, Combust. Theory Model 18 (1) (2014) 65–88.

[12] H. Barths, C. Hasse, N. Peters, Computational fluid dynamics modelling of non-premixed combustion in direct injection diesel engines, Int. J. Eng. Res. 1 (3) (2000) 249–267.

[13] Z. Luo, S. Som, S.M. Sarathy, M. Plomer, W.J. Pitz, D.E. Longman, T. Lu, Development and validation of an n-dodecane skeletal mechanism for spray combustion applications, Combust. Theory Model. 18 (2) (2014) 187–203.

[14] E. Ranzi, P. Gaffuri, T. Faravelli, P. Dagaut, A wide-range modeling study of n-heptane oxidation, Combust. Flame 103 (1–2) (1995) 91–106.

[15] E. Ranzi, A. Frassoldati, R. Grana, A. Cuoci, et al., Hierarchical and comparative kinetic modeling of laminar flame speeds of hydrocarbon and oxygenated fuels, Prog. Energy Combust. Sci. 38 (4) (2012) 468–501.

[16] P. Dagaut, A. Ristori, A. Frassoldati, T. Faravelli, et al., Experimental and semi-detailed kinetic modeling study of decalin oxidation and pyrolysis over a wide range of conditions, Proc. Combust. Inst. 34 (1) (2013) 289–296.

[17] A. Frassoldati, R. Grana, T. Faravelli, E. Ranzi, et al., Detailed kinetic modeling of the combustion of the four butanol isomers in premixed low-pressure flames, Combust. Flame 159 (7) (2012) 2295–2311.

[18] M.R. Djokic, K.M. Van Geem, C. Cavallotti, A. Frassoldati, E. Ranzi, G.B. Marin, An experimental and kinetic modeling study of cyclopentadiene pyrolysis: first growth of polycyclic aromatic hydrocarbons, Combust. Flame 161 (11) (2014) 2739–2751.

[19] E. Ranzi, A. Frassoldati, A. Stagni, M. Pelucchi, A. Cuoci, T. Faravelli, Reduced kinetic schemes of complex reaction systems: fossil and biomass-derived transportation fuels, Int. J. Chem. Kinet. 46 (2014) 512–542, doi:10.1002/kin.20867.

[20] R. Grana, A. Frassoldati, C. Saggese, T. Faravelli, E. Ranzi, A wide range kinetic mod-eling study of pyrolysis and oxidation of methyl butanoate and methyl decanoate
- Note II: lumped kinetic model of decomposition and combustion of methyl esters up to methyl decanoate, Combust. Flame 159 (7) (2012) 2280–2294.

[21] M. Mehl, T. Faravelli, E. Ranzi, T. Lucchini, A. Onorati, F. Giavazzi, P. Scorletti, D. Terna, Kinetic Modeling of Knock Properties in Internal Combustion Engines, SAE Paper 2006-01-3239, 2006.

[22] M. Mehl, T. Faravelli, F. Giavazzi, E. Ranzi, P. Scorletti, A. Tardani, D. Terna, Detailed chemistry promotes understanding of octane numbers and gasoline sensitivity, Energy Fuels 20 (6) (2006) 2391–2398.

[23] G. D'Errico, T. Lucchini, A. Onorati, M. Mehl, T. Faravelli, E. Ranzi, S. Merola, B.M. Vaglieco, Development and Experimental Validation of a Combustion Model with Detailed Chemistry for Knock Predictions, SAE Paper 2007-01-0938 (2007).

[24] M. Mehl, A. Tardani, T. Faravelli, E. Ranzi, G. D'Errico, T. Lucchini, A. Onorati, D. Miller, N. Cernansky, A Multizone approach to the detailed kinetic modeling of HCCI combustion, SAE Paper 2007-24-0086 (2007).

[25] K. Narayanaswamy, P. Pepiot, H. Pitsch, A chemical mechanism for low to high temperature oxidation of n-dodecane as a component of transportation fuel sur-rogates, Combust. Flame 161 (2014) 866–884.

[26] H. Wang, Y. Ra, M. Jia, R.D. Reitz, Development of a reduced n-dodecane-PAH mechanism, and its application for n-dodecane soot predictions, Fuel 136 (2014) 25–36.

[27] S.M. Sarathy, C.K. Westbrook, M. Mehl, W.J. Pitz, C. Togbe, P. Dagaut, H. Wang,
M.A. Oehlschlaeger, U. Niemann, K. Seshadri, P.S. Veloo, C. Ji, F.N. Egolfopoulos, T. Lu, Comprehensive chemical kinetic modeling of the oxidation of 2-methylalkanes from C7 to C20, Combust. Flame 158 (2011) 2338–2357.

[28] C.K. Westbrook, W.J. Pitz, O. Herbinet, H.J. Curran, E.J. Silke, A comprehensive detailed chemical kinetic reaction mechanism for combustion of n-alkane hydrocarbons from n-octane to n-hexadecane, Combust. Flame 156 (2009) 181–199.

[29] T.F. Lu, C.K. Law, A directed relation graph method for mechanism reduction, Proc. Combust. Inst. 30 (2005) 1333–1341.

[30] W. Liu, R. Sivaramakrishnan, M.J. Davis, S. Som, D.E. Longman, T. Lu, Development of a reduced biodiesel surrogate model for compression ignition engine modeling, Proc. Combust. Inst 34 (1) (2013) 401–409.

[31] X.L. Zheng, T.F. Lu, C.K. Law, Experimental counterflow ignition temperatures and reaction mechanisms of 1,3-butadiene, Proc. Combust. Inst. 31 (1) (2007) 367–375.

[32] P. Pepiot-Desjardins, H. Pitsch, An efficient error propagation based reduction method for large chemical kinetic mechanisms, Combust. Flame 154 (2008) 67–81.

[33] P. Pepiot-Desjardins, H. Pitsch, An automatic chemical lumping method for the reduction of large chemical kinetic mechanisms, Combust. Theory. Mod 12 (6) (2008) 1089–1108.

[34] S.S. Vasu, D.F. Davidson, Z. Hong, V. Vasudevan, R.K. Hanson, n-Dodecane oxidation at high-pressures: measurements of ignition delay times and OH concentration time-histories, Proc. Combust. Inst. 32 (1) (2009) 173–180.

[35] H.S. Shen, J. Steinberg, J. Vanderover, M.A. Oehlschlaeger, A shock tube study of the ignition of n-heptane, n-decane, n-dodecane, and n-tetradecane at elevated pressures, Energy Fuels 23 (5) (2009) 2482–2489.

[36] D.F. Davidson, Z. Hong, G.L. Pilla, A. Farooq, R.D. Cook, R.K. Hanson, Multispecies time history measurements during n-dodecane oxidation behind reflected shock waves, Proc. Combust. Inst 33 (2011) 151–157.

[37] D.F. Davidson, D.R. Haylett, R.K. Hanson, Development of an aerosol shock tube for kinetic studies of low-vapor-pressure fuels, Combust. Flame 155 (2008) 108–117.

[38] T. Malewicki, K. Brezinsky, Experimental and modeling study on the pyrolysis and oxidation of n-decane and n-dodecane, Proc. Combust. Inst. 34 (1) (2013) 361–368.

[39] R.D. Wilk, R.S. Cohen, N.P. Cernansky, Ignition studies of dodecane and binary mixtures of dodecane and tetralin, in: Proceedings of the Twentieth Symposium (International) on Combustion, 1984, pp. 187–193.

[40] P.S. Veloo, S. Jahangirian, F.L. Dryer, An experimental and kinetic modeling study of the two stage autoignition kinetic behavior of C7, C10, C12, and C14 n-alkanes, in: Proceedings of the Spring Technical Meeting, Central States Section of the Combustion Institute, April 22nd–24th, 2012.

[41] M.S. Kurman, R.H. Natelson, N.P. Cernansky, D.L. Miller, Speciation of reaction intermediates from n-dodecane oxidation in the low temperature regime, Proc. Combust. Inst. 33 (1) (2011) 159–166.

[42] A. Mzé-Ahmed, K. Hadj-Ali, P. Dagaut, G. Dayma, Experimental and modeling study of the oxidation kinetics of n-undecane and n-dodecane in a jet-stirred reactor, Energy Fuels 26 (7) (2012) 4253–4268.

[43] O. Herbinet, P.-M. Marquaire, F. Battin-Leclerc, R. Fournet, Thermal decomposition of n-dodecane: Experiments and kinetic modeling, J. Anal. Appl. Pyrolysis 78 (2007) 419–429.
[44] K. Kumar, C.-J. Sung, Laminar flame speeds and extinction limits of preheated n-decane/O2/N2 and n-dodecane/O2/N2 mixtures, Combust. Flame 151 (1) (2007) 209–224.
[45] C. Ji, E. Dames, Y.L. Wang, H. Wang, F.N. Egolfopoulos, Propagation and extinction of premixed C5 to C12 n-alkane flames, Combust. Flame 157 (2010) 277–287.
[46] X. Hui, C.-J. Sung, Laminar flames speeds of transportation-relevant hydrocarbons and jet fuels at elevated temperatures and pressures, Fuel 109 (2013) 191–200.
[47] M. Tanabe, C. Bolik, C. Eigenbrod, H.J. Rath, J. Sato, M. Kono, Spontaneous ignition of liquid droplets from a view of non-homogeneous mixture formation and transient chemical reactions, in: Proceedings of the Twenty-Sixth Symposium (International) on Combustion, The Combustion Institute, 1996, pp. 1637–1642.
[48] A. Cuoci, A. Frassoldati, T. Faravelli, E. Ranzi, OpenSMOKE++: An object-oriented framework for the numerical modeling of reactive systems with detailed kinetic mechanisms, Compu. Phys. Commun. 192 (2015) 237–264.
[49] G. Borghesi, E. Mastorakos, Spontaneous ignition of isolated n-heptane droplets at low, intermediate, and high ambient temperatures from a mixture-fraction perspective, Combustion and Flame 162 (2015) 2544–2560.
[50] A. Cuoci, M. Mehl, G. Buzzi-Ferraris, T. Faravelli, D. Manca, E. Ranzi, Combust. Flame 143 (3) (2005) 211–226.
[51] A. Cuoci, A. Frassoldati, T. Faravelli, E. Ranzi, Numerical modeling of auto-ignition of isolated fuel droplets in microgravity, Proc. Combust. Inst. 35 (2) (2015) 1621–1627.
[52] C. Saggese, N.E. Saánchez, A. Frassoldati, A. Cuoci, T. Faravelli, M.U. Alzueta, E. Ranzi, Kinetic modeling study of polycyclic aromatic hydrocarbons and soot formation in acetylene pyrolysis, Energy Fuels 28 (2014) 1489–1501.
[53] C. Saggese, A. Frassoldati, A. Cuoci, T. Faravelli, E. Ranzi, A wide range kinetic modeling study of pyrolysis and oxidation of benzene, Combust. Flame 160 (2013) 1168–1190.
[54] T. Lucchini, G. D'Errico, D. Ettorre, F. Brusiani, G.M. Bianchi, A. Montanaro, L. Allocca, Experimental And Numerical Investigation of High-Pressure Diesel Sprays with Multiple Injections at Engine Conditions, SAE Technical Paper 2010-01-0179 (2010).
[55] F. Contino, H. Jeanmart, T. Lucchini, G. D'Errico, Coupling of in situ adaptive tabulation and dynamic adaptive chemistry: an effective method for solving combustion in engine simulations, Proc. Combust. Inst. 33 (2) (2011) 3057–3064.
[56] T. Lucchini, G. D'Errico, D. Ettorre, Numerical investigation of the spray mesh tur-bulence interactions for high-pressure, evaporating sprays at engine conditions, Int. J. Heat Fluid Flow 32 (1) (2011) 285–297.
[57] R.D. Reitz, Modeling atomization processes in high pressure vaporizing sprays, At. Spray Technol. 3 (1987) 309–337.
[58] C. Bajaj, M. Ameen, J. Abraham, Evaluation of an unsteady flamelet progress variable model for autoignition and flame lift-off in diesel jets, Combust. Sci. Technol. 185 (2013) 454–472.
[59] C. Bekdemir, Somers, L.L. Goeyde, Modeling diesel engine combustion using pressure dependent flamelet generated manifolds, Proc. Combust. Inst. 33 (2011) 2887–2894.
[60] G. De Paola, E. Mastorakos, Y.M. Wright, K. Boulouchos, Diesel engine simulations with multi-dimensional conditional moment closure, Combust. Sci. Technol. 180 (5) (2008) 883–899.
[61] M. Bolla, D. Farrace, Y.M. Wright, K. Boulouchos, E. Mastorakos, Influence of turbulence–chemistry interaction for n-heptane spray combustion under diesel engine conditions with emphasis on soot formation and oxidation, Combust. The-ory Model. 18 (2) (2014) 330–360.
[62] Y. Pei, E.R. Hawkes, S. Kook, G.M. Goldin, T. Lu, Modelling n-dodecane spray and combustion with the transported probability density function method, Combust. Flame 162 (5) (2015) 2006–2019.
[63] S. Bhattacharjee, D.C. Haworth, Simulations of transient n-heptane and n-dodecane spray flames under engine-relevant conditions using a transported PDF method, Combust. Flame 160 (2013) 2083–2102.
[64] http://www.sandia.gov/ecn/workshop/ECN3/ECN3_Topic2.2-FlameStructure_Final.pptx (accessed 01.07.15).
[65] S.A. Skeen, J. Manin, L.M. Pickett, Simultaneous formaldehyde PLIF and high-speed schlieren imaging for ignition visualization in high-pressure spray flames, Proc. Combust. Inst. 35 (3) (2015) 3167–3174.
[66] C.A. Idicheria, L.M. Pickett, Quantitative mixing Measurements in a Vaporizing Diesel Spray by Raileigh Imaging, SAE Paper 2007-01-0647 (2007).